The Study of Surface & Subsurface Characteristics of Volcanic Region on Mars using Remote Sensing & GIS

Thesis submitted

To

Gujarat University

For the Degree of

Doctor of Philosophy in Geoinformatics

By

RAJIV RANJAN BHARTI

Under the Guidance of

Prof. Neeraj Srivastava
(Guide)
Associate Professor
(Head, Planetary Remote Sensing Section)
Planetary Science Division,
Physical Research Laboratory
Ahmedabad -380 009
Gujarat, India

Prof. Shital H Shukla
(Co-Guide)
Associate Professor
(Head of Department)
Department of Earth Sciences
Gujarat University
Ahmedabad -380 009
Gujarat, India

Department of Earth Sciences
University School of Science
Gujarat University
Ahmedabad 380009

Submitted on: 24/06/2024

Registration No.: 9142 **Registration Date: 13/08/2019**

“To my Mother and Father, in loving memory"

Declaration

I declare here that the thesis entitled **"The Study of Surface & Subsurface Characteristics of Volcanic Region on Mars using Remote Sensing & GIS"** to the award of the Degree of Doctor of Philosophy in Geoinformatics from the Department of Earth Sciences, Gujarat University is my original work and contains no plagiarism. The research was carried out during the period from August 13th, 2019, to June 19th, 2024 under the guidance of Prof. Neeraj Srivastava (Guide) and Prof. Shital Shukla (Co-Guide). Additionally, to the best of my knowledge, I certify that the information I acquired from other sources has been properly acknowledged.

Date: 19/06/2024 **(Rajiv Ranjan Bharti)**

Place: Ahmedabad Reg. No. 9142/13-08-2019

Certificate

This is to certify that the thesis entitled **"The Study of Surface & Subsurface Characteristics of Volcanic Region on Mars using Remote Sensing & GIS,"** submitted by Rajiv Ranjan Bharti, is his original research contribution for the award of the Degree of Philosophy in Geoinformatics from the Department of Earth Sciences, Gujarat University. The research was carried out under my supervision from August 13th, 2019, to June 19th, 2024. He has complied with all rules and specifications set forth by Gujarat University in order to submit the thesis. The content of the thesis, in full or in part, has not been submitted to any other Institute or University for the award of any other degree or diploma.

Date: 19/06/2024 **(Rajiv Ranjan Bharti)**

Place: Ahmedabad Reg. No. 9142/13-08-2019

Prof. Neeraj Srivastava
(Guide)
Associate Professor
(Head, Planetary Remote Sensing Section)
Planetary Science Division
Physical Research Laboratory
Navrangpura,
Ahmedabad -380 009,
Gujarat, India

Prof. Shital H Shukla
(Co-Guide)
Associate Professor
(Head of Department)
Department of Earth Sciences,
Gujarat University
Navrangpura,
Ahmedabad -380 009,
Gujarat, India

Acknowledgements

This thesis would not have been possible without the guidance and help of several individuals who, in one way or another, contributed and extended their valuable assistance in the preparation and completion of this study. It is a pleasure to thank those who made it possible.

The research environment in the Physical Research Laboratory has worked as a catalyst for me to do a Ph.D. I enrolled myself as a Ph.D. student in the Department of Earth Sciences, Gujarat University, and carried out my research work at PRL under my supervisor, Prof. Neeraj Srivastava, Head, Planetary Remote Sensing, Planetary Science Division, Physical Research Laboratory (PRL) and Prof. Shital Shukla, HOD, Department of Earth Sciences, Gujarat University. I would like to express my sincere gratitude to my supervisors for their invaluable guidance and support throughout this research project. Their expertise and mentorship have been instrumental in my academic growth. I would also like to express my sincere gratitude to DPC members Dr. D. Ram Rajak and Dr. Sandeep Pandey for time-to-time encouragement and critical review remarks, which helped me to improve the quality of the work done in this research work.

I would like to express my sincere gratitude to Prof. Anil Bhardwaj, Director PRL, and Prof. Varun Sheel, Chairman, Planetary Science Division, PRL; without their support, this PhD would have never been completed.

I would like to thank Prof. S.V.S Murty, Ex. Chairman of the Planetary Science Division, who encouraged me to initiate research work on the Martian subsurface.

I also express my sincere gratitude to Dr. Shiv Mohan (SAC) and Dr. Than Putzig (PSI, Colorado, USA). I understood the basics of SHARAD from them and started research work on the Martian subsurface using SHARAD data.

I also thank the International Astronomical Union (IAU) for giving the names of the three craters which have been studied in this thesis. On the recommendation of the PRL, the International Astronomical Union (IAU) Working Group for Planetary System Nomenclature approved naming the three craters on Mars as follows: Lal crater (based on former Director of PRL, Mursan crater (based on a town in Uttar Pradesh) and Hilsa crater (A town in Bihar).

One more important incident, which I wish to discuss here because it is very important for my research career. I received an invitation to attend the MARSIS and SHARAD science team meeting, which was held in Grenoble, France, in 2018. Dr. Than Putzig introduced me to several renowned scientists at NASA and ESA. During this meeting, I understood new techniques and their ideas, which led me to think differently to do new science. He introduced me to Dr. Isaac Smith, Co-PI of the MRO's SHARAD instrument. Dr. Isaac, now my friend, gave unconditional support and time to my research work. I learned many new techniques to study the subsurface of Mars from him. As a result of close collaboration, we could do exciting science and continue to work together on different projects.

I owe a deep sense of gratitude to Dr. Sanjay Kr. Mishra and Dr. Rishitosh Sinha. They are my colleague and friends with whom I always discuss science to general topics, and they give me a sense of relief from my

busy schedule. I also thank my friends, Alok and Hitendra, who were always curious to know about the status of my thesis work.

Lastly, I want to express my deepest gratitude to my wife, Anjusha. Thank you for always being my rock, accompanying me through the highs and lows of this academic journey. Your support and belief in me have been a source of strength and motivation. To my wife, daughter, and son: Thank you for everything. I dedicate this PhD thesis to you.

Announcement

The International Astronomical Union (IAU) has approved the PRL proposal for the naming of the craters which is studied in this thesis. Hence, the name of the crater used in this thesis is as per the IAU nomenclature. Details are following:

Approved by International Astronomical Union (IAU)

Subject: Re: Naming an unnamed crater on Mars (Lal, Mursan, and Hilsa Approved)

From: "Gaither, Tenielle A" <tgaither@usgs.gov>

Date: Thu, June 6, 2024 2:04 am

To: "rajiv@prl.res.in" <rajiv@prl.res.in>

Cc: "Nomenclature, GS-ASC Astro" <gs-astro_nomenclature@usgs.gov>

Priority: Normal

Options: View Full Header | View Printable Version | Download this as a file | View Message details | Add to Address Book

Dear Rajiv,

The IAU Working Group for Planetary System Nomenclature has approved the names
Lal<https://planetarynames.wr.usgs.gov/Feature/16288>,
Mursan<https://planetarynames.wr.usgs.gov/Feature/16289>, and
Hilsa<https://planetarynames.wr.usgs.gov/Feature/16290> for these three craters on
Mars. The names may now be used in papers, presentations, and maps.

Thank you for your patience during the review process, and let me know if you have any questions.

Best regards,

Tenielle

Three Carters on Mars Discovered by PRL Scientist:
International Astronomical Union (IAU) named them after the PRL Former Director and two small towns in India

The scientists of Physical Research Laboratory (PRL) in Ahmedabad, a Unit of Department of Space, Govt. of India, have discovered three new craters on Mars around the 21.0 S, 209 W. These craters are situated in the Tharsis volcanic region on Mars. On the recommendation of the PRL, the International Astronomical Union (IAU) Working Group for Planetary System Nomenclature approved naming the three craters on Mars as following:

1. **Lal crater:** <https://planetarynames.wr.usgs.gov/Feature/16288>
It is about 65 km wide crater, centered at -20.98° and 209.34°.
The name is given after the renowned Indian geophysicist and former Director of PRL, Prof. Devendra Lal. He was the director of PRL during 1972-1983.
About Prof.Lal : https://www.geochemsoc.org/news/2012/12/14/devendra-lal-1929-2012

2. **Mursan crater:** <https://planetarynames.wr.usgs.gov/Feature/16289>
It is a ~10 km wide crater and superimposed on the eastern side of the rim of the Lal crater. It is named after a town in Uttar Pradesh, India.

3. **Hilsa crater:** <https://planetarynames.wr.usgs.gov/Feature/16290>
It is also a ~10 km wide crater and superimposed on the western side of the rim of the Lal crater. It is named after a town in Bihar, India.

Scientific importance:
The entire area of Lal crater, in the Tharsis volcanic region on Mars, is covered with lava. There are geophysical evidence of material other than lava in this crater, with a 45-m thick sedimentary deposit in the subsurface of the crater, obtained using subsurface radar SHARAD/MRO. This discovery provides compelling evidence that the water has moved large volumes of sediment into the crater now named as "Lal Crater". This finding also confirms that Mars was once wet and water has flown on the surface. Two small superimposed craters, on either side of Lal Crater, named as Mursan and Hilsa, provide the timeline for the infilling process of the Lal Crater and suggest that the infilling has been episodic.

Link to the scientific article:

Bharti, R. R., Smith, I. B., Mishra, S. K., Srivastava, N. & Shukla, S. H. SHARAD detection of sedimentary infilling within an unnamed crater near Mangala Fossa region, Mars, *Icarus,* **371**, 114713 (2022). https://doi.org/10.1016/j.icarus.2021.114713

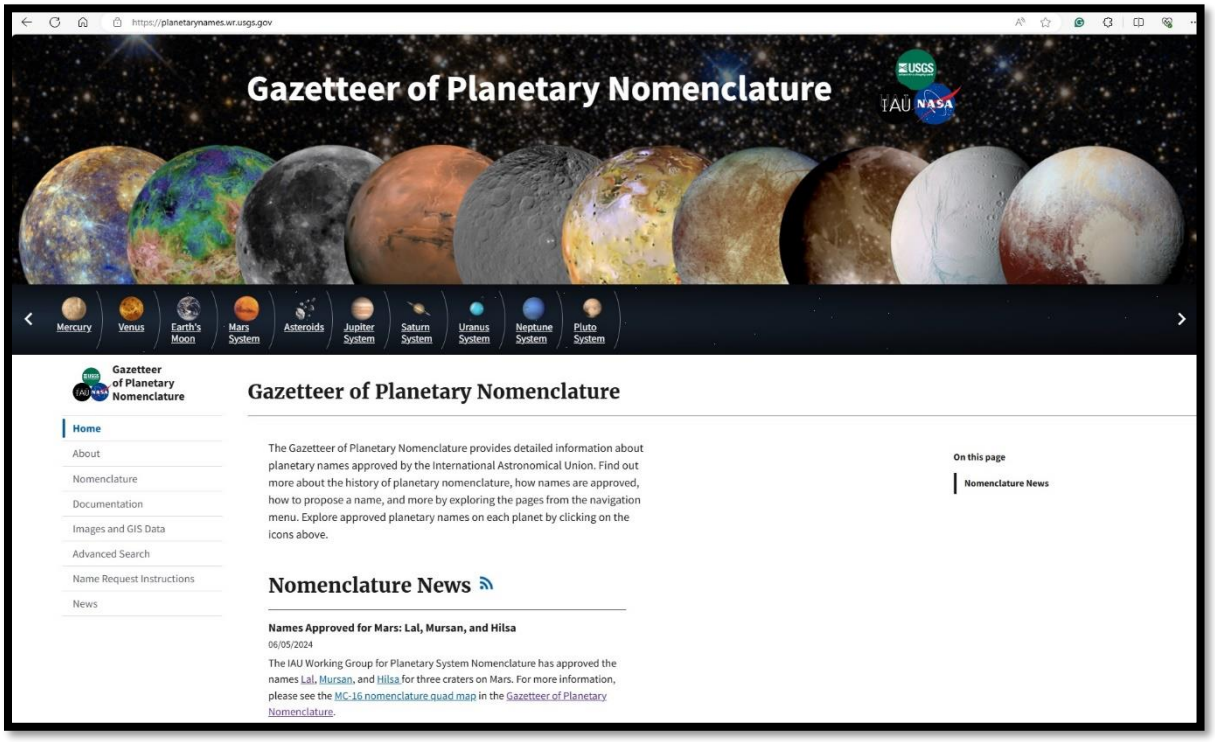

Gazette notification by United States Geological Survey (USGS)

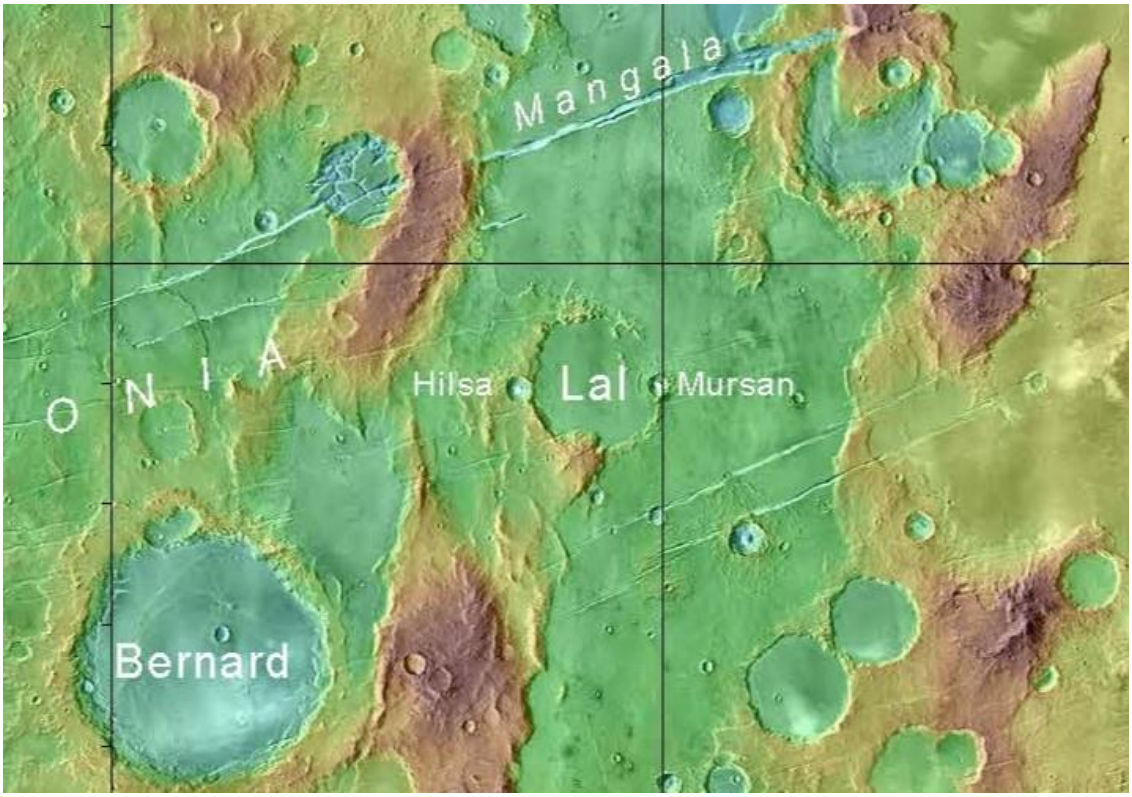

Caption: The location of the Lal, Mursan, and Hilsa craters on Mars
https://asc-planetarynames-data.s3.us-west 2.amazonaws.com/mc16_2014.pdf

Abstract

Exploration of the solar system has provided immense opportunities for research on the geologic evolution of planets. Various geological activities shape a planetary body; however, volcanic activity is particularly important for providing insights in terms of composition and thermal evolution of the planetary bodies. With the advancement of space technology, we have high-resolution spacecraft imageries and subsurface data of rocky planets, which reveal an array of volcanic landforms. These different volcanic landforms give us an opportunity to understand the magmatic process and petrology of the planetary bodies.

The western hemisphere of Mars is dominated by a massive volcano-tectonic complex known as the Tharsis region or the Tharsis bulge. This immense, elevated structure is thousands of kilometers in diameter and it covers up to 25% of the planet's surface. Graben systems, outflow channels, and infilled craters are the most common landforms in this region. The study of these landforms using remote sensing data and GIS tools is important to understand the evolution of the planet Mars.

Infilled craters are important morphological structures for understanding the past geological history. In this thesis, the subsurface of an infilled crater, "Lal" (IAU approved name), centered at 21.0° S, 150.6° W has been studied for the first time using Shallow Radar (SHARAD) based observations. It is situated south of the Mangala Fossa and Mangala Valles, a major fluvial outflow channel system. In contrast to the adjacent Tharsis lava flows, the analysis of radar propagation in the Lal crater reveals a low loss tangent (0.008–0.009) and lower dielectric subsurface material (average

5.6) for a subsurface unit that is ~40 m thick. These values are unexpected in this region. Lava flows dominate the surface and the surrounding region, and SHARAD investigations of lava flows in the Tharsis region have detected higher values, creating a discrepancy that is discussed in this thesis. The observed stratigraphy and the subsurface geophysical properties suggest that the crater infilling is composed of moderate-density sedimentary material buried by a layer of lava in the eastern portion of the Lal crater. Two small superimposed craters on either side of Lal crater- Mursan and Hilsa- provide the timeline for the infilling process of the Lal crater and suggest that the infilling has been episodic. The measurements also support the previous geologic mapping of the region where the present day surface material comprises of undifferentiated impact, volcanic, fluvial, and basin materials. In this study, two subsurface reflections have been identified and examined for clues to determine whether one of the layers is sediment rather than lava. The detection of two layers of subsurface reflections also indicates that the infilling occurred in at least four successive events. These results are significant because they add more context to this region and provide compelling evidence that water moved large volumes of sediment into this basin.

The second major geomorphological feature in the volcanic region of Mars is massive graben systems, which occur as extensive linear cracks. They cover a region more than 8,000 km in diameter and nearly one-third of the planet's circumference. Many of them trend radially outward from the Tharsis Montes. They are long-lived crucial features to determine the evolution of tectonism and volcanism on Mars. Thousands of grabens were discovered in the early 1970s and have been studied extensively with different hypotheses about their formation throughout the literature. These

hypotheses include the formation process being either tectonic or a combination of tectonic and magmatic processes, but no consensus has been reached so far. In this study, the subsurface of narrow graben systems has been explored for the first time using SHARAD data to understand their formation mechanism. Multiple subsurface reflections has been observed in a narrow range of time delay at the rim of Mangala Fossa and at the floor of the Labeatis Fossa. The loss tangent of the subsurface unit is in the range of 0.009 to 0.03, consistent with low to moderate-density basalt. The presence of a basaltic subsurface unit at these locations confirms that magmatism is involved during the formation of these two graben systems.

The subsurface reflections at these two widely separated locations on Mars are reported in this thesis for the first time. They reveal new insights to understand the volcanic region on Mars. The presence of subsurface sedimentary deposits in a lava-covered region and lava deposits at the rim of Mangala Fossa and the floor of Leabits Fossa reveal that the volcanic region experienced diverse geological activities throughout the Martian evolution. The sedimentary deposit in the subsurface of Lal crater confirmed that the fluvial activities were an active process during the Martian past, and the lava deposit on the rim of Mangala Fossa and at the floor of Leabitis Fossa suggests that the volcanism helped in the formation of the magnificent graben systems that shaped the red planet.

Contents

List of Figures and Tables

List of Figures

List of Tables

Abbreviations

AHi	Amazonian and Hesperian impact unit;
AHv	Amazonian and Hesperian volcanic unit;
ArcGIS	Aeronautical Reconnaissance Coverage Geographic Information System
ASU	Arizona State University
CO-SHARP	Colorado SHARAD processing system
CTX	Context camera
dB/μs	Decibel per microsecond
DEM	Digital elevation model
DOS	Department of Space
ε	Dielectric Constant
eHv	Early Hesperian volcanic unit
em	Electromagnetic
eNh	Noachian highland unit
ENVI	Environment for Visualising Images)
ESA	European Space Agency
GIS	Geographic information system
HRSC	High-Resolution Stereo Camera
IAU	International Astronomical Union
INh	Late Noachian highland unit
ISRO	India Space Research Organization
JMARS	java Mission-planning and Analysis for Remote Sensing
JPL	Jet Propulsion Laboratory
MARSIS	Mars Advanced Radar for Subsurface and Ionosphere Sounding

MCC	Mars Color Camera
MGS	Mars Global Surveyor
MLE	Multi Layered ejecta
MNh	Middle Noachian highland unit.
MOLA	Mars Orbiter Laser Altimeter HRSC High-resolution stereo camera
MOM	Mars Orbiter Mission
MRO	Mars Reconnaissance Orbiter
NASA	National Aeronautics and Space Administration
NPLD	North Polar Layer Deposit
PDS	Planetary Data System
PRL	Physical Research Laboratory
P_s	Power Surface
P_{ss}	Power Subsurface
QGIS	Quantum geographic information system
sgy	Seismic Expert Group
SHARAD	Shallow radar
twt	Two Way Time
THEMIS	Thermal Emission Imaging System
USGS	United States Geological Survey
VBF	Vastitas Borealis Formation

"If you want to shine like a sun, first burn like sun"
- APJ Abdul Kalam

Chapter 1

Introduction

1.1 Why we explore Mars?

The red planet Mars has always captivated humans since we first recognized it through bare eyes. The first telescope observation, in 1877, revealed intriguing surface features, and many thought they were evidence of civilization on Mars. From further advancements in observation, people came to know that there is no artificial construction on Mars, but scientists also learned that billions of years ago, the present-day dry and hostile planet might have once been as habitable as Earth (McKay and Stoker, 1989). Many features on Mars, like branching streams, river valleys, basins, and deltas, which exist on the Earth as well revealed that Mars once had a vast ocean covering the northern hemisphere and a thick atmosphere that maintained liquid water on the surface.

During the evolution of Mars, something happened that dramatically transformed the planet that was once rather Earth-like into the dusty, dry husk we see today. The question is what happened? Where did those liquids go, and what happened to the Martian atmosphere? Different hypotheses are given to understand this transformation, and the community is still working on it. This is important to know so that we can leverage our knowledge to understand our precious planet Earth and its atmosphere and mitigate the impacts of climate change on Earth. For example, NASA's Curiosity observed a preserved stream-bed like the one we find on Earth and it helps to understand that there was standing water on the surface of Mars during the period of the planet's history. It shows clearly the planet had a completely different atmosphere and climate than it possesses today. What are the reasons behind this transition that once

there was surface water but now it is a barren land? This change is important to understand so that we can mitigate the impact of climate change on Earth. One another example, if our experiment successfully grows a plant on Mars, we can use that knowledge to grow a plant on the Earth in extreme conditions. These are a select few justifications in favor of studying Mars. Rightly said, "Space exploration is embedded into the foundation of our past, exists at the forefront of the present, and is inevitable in our society's future" (Bains Jay, 2022).

1.2 The exploration approach

Four scientific approaches are used by scientists to understand the planet Mars:

- **Earth-based radar:** Arecibo Observatory mapped the Mars surface using the radio telescope. Now, it is decommissioned in 2020.
- **Orbiter/ Fly-By:** Orbiter / Fly-By mission based instruments are used to probe the atmosphere and surface of Mars through remote sensing. MOM (2014), Mars Odyssey (2001), Mars Express (2003), and MRO (2005) are a few important orbiter missions to Mars.
- **Lander:** This approach is used for in situ measurement of soil and atmosphere in one place. It started with Vikings 1(1975) and 2 (1975) and moved to InSight Lander (2018), which were used to probe the surface, subsurface, and atmosphere of Mars.

- **Rover:** Mobile vehicle loaded with suite of instruments is used to probe and analyze the surface and atmosphere of Mars. Sprit (2004), Opportunity (2004), Pathfinder (1997), Curiosity (2020), Mars Science Laboratory (2012), and the Mars 2020 Perseverance Rover are the important rover missions to Mars.

All the above approaches, except the orbiter, have limited range. Orbiter or Satellite remote sensing technology proves to be an excellent tool for inventory and monitoring due to its wide coverage and revisit capability, therefore large amount of information is gathered from orbiter satellite data. These data helps us to understand the different geological activities on Mars, and it also helps us to understand the chronology of these geological activities.

1.3 Chronology of geological processes on Mars

Volcanic processes on Mars have been active over more than 4 Gyr, with peak phases in all three geologic epochs, generally ceasing towards the Amazonian. Fluvial and lacustrine activity phases spread a time span from Noachian until Amazonian times, but detailed studies show that they have been interrupted by multiple and long lasting phases of quiescence. Also glacial activity shows discrete phases of enhanced intensity that may correlate with periods of increased spin-axis obliquity. The episodicity of geological processes like volcanism, erosion, and glaciation on Mars reflects close correlation between surface processes and endogenic activity as well as orbit variations and changing climate condition (Jaumann., 2015). In the absence of in situ data from Martian soil (samples), the only way to

determine the relative ages of several regions is to count the craters that mark them (Hartmann and Neukum, 2001). Based on this technique, stages of geological processes are defined in three epochs: Noachian, Hesperian, and Amazonian. Figure 1.1 broadly represents the major geological activities vis. volcanism, tectonism and fluvial activities in chronological order.

	Timeline	Volcanism	Tectonics / Cratering	Fluvial Activities
3.0 Ga	Amazonian	▪ Decline of volcanic activities from all areas. ▪ Lava flows in southern Elysium Planitia. ▪ Large flows in the Elysium region.	▪ Tectonics activities in Tharsis. ▪ Formation of Elysium Fossae. ▪ Initial formation of halo deposits of Olympus Mons.	▪ Gullies formation
3.7 Ga	Hesperian	▪ Volcanism in Tempe Terra and Syrtis Major. ▪ Major volcanism in the Elysium and Tharsis regions.	▪ Formation of Noctis Labyrinthus. ▪ Valles Marineris Formation. ▪ Formation of large wrinkle networks.	▪ Formation of outflow channels ▪ Filling of northern plains.
4.1 Ga	Noachian	▪ Tharsis Bulge. ▪ Beginning of volcanism in highlands.	▪ Formation of Ceraunius, Tempe, and Noctis Fossae. ▪ Impact craters.	▪ Formation of vast valley networks and fluvial branches.

Figure 1.1 Chronology of geological activities on Mars. Adopted from Head et al., 2001 and Cyril Grima, 2011.

From the above chronology of geological activities, it can be seen that volcanism and tectonism were active throughout the Martian history, and both are complemented by each other. Considering this fact, my thesis broadly covers these two geological activities and their implications in our understanding of volcanic regions on Mars.

1.4 Volcanism on Mars

Volcanic activity or volcanism is a significant geological process that shaped the planetary bodies like Moon, Mercury, Venus, and Mars. In this igneous process, the eruption of molten rock (magma) onto the surface of a solid-surface planet can produce flat lava plains or a wide variety of topographic features.

Mars displays a range of volcanic features ranging in the ages from Noachian to late Amazonian, with major volcanic activity concentrated in the Tharsis and Elysium regions (Hodges and Moore, 1994) (Figure 1.2). The huge shield of volcanoes on Mars, including enormous channels and canyons, was the striking discovery of the Mariner 9 in 1971 (Masursky et al., 1972; McCauley et al., 1972; Carr, 1973, 1976b). Among them, the Tharsis region has the largest concentration of Martian volcanoes, with 12 large volcanoes, many smaller features, and extensive lava flows. The Tharsis Bulge occupies about 25% of the surface and rises about 6 km above the mean planetary radius (Anderson et al., 2001; Phillips et al., 2001; Smith et al., 2001a). In other words, these volcanoes and associated lava flows cover around 18 million km^2 and rise more than 25 km above the datum_level (Scott and Tanaka, 1981). The formation of this enormous volcanic province happened during the Noachian (~4.1–3.5 billion years ago, Ga) and Hesperian (~3.5–3.2 Ga) epochs (Carr and Head, 2010). It has three giant volcanoes, Arsia Mons, Pavonis Mons, and Ascraeus Mons, aligned northeast-south-west across the equator. Olympus Mons, on the north-western flank of the Tharsis, is the largest known volcano in the Solar

System, with a base diameter of about six hundred kilometers and a summit rising twenty-five kilometers above the surrounding plains.

The other large volcano in the Tharsis region is 1600 km diameter Alba Patera, located on the northern edge of the Tharsis uplift. Alba Patera is surrounded by circumferential systems of graben systems. The summit caldera rises to 6.8 km in height (Cattermole, 1990; Schneeberger and Pieri, 1991).

The Elysium Volcanic Province is the second-largest volcanic province on Mars. The lava flows in this region show model ages ranging from 3.4 Ga to 60 Ma (Platz and Michael, 2011). It is located on a broad dome about two thousand kilometers across the mid-latitude plains of the northern hemisphere. The two large shield volcanoes here, known as Elysium Mons and Hecates Tholus, are significantly smaller than those of the Tharsis bulge.

Flood basalts are common, as are lava plains surrounding the big volcanoes in the Tharsis and Elysium regions. It occurred throughout the Martian history (McEwen et al., 1999), but their extent has decreased over time with the decline of volcanic activities. These lava-covered regions have diversified morphological features. Infilled craters, multilayer ejecta craters, pit craters, linear graben systems, and outflow channels are some prominent morphological features of these regions. These features are briefly explained in the next section.

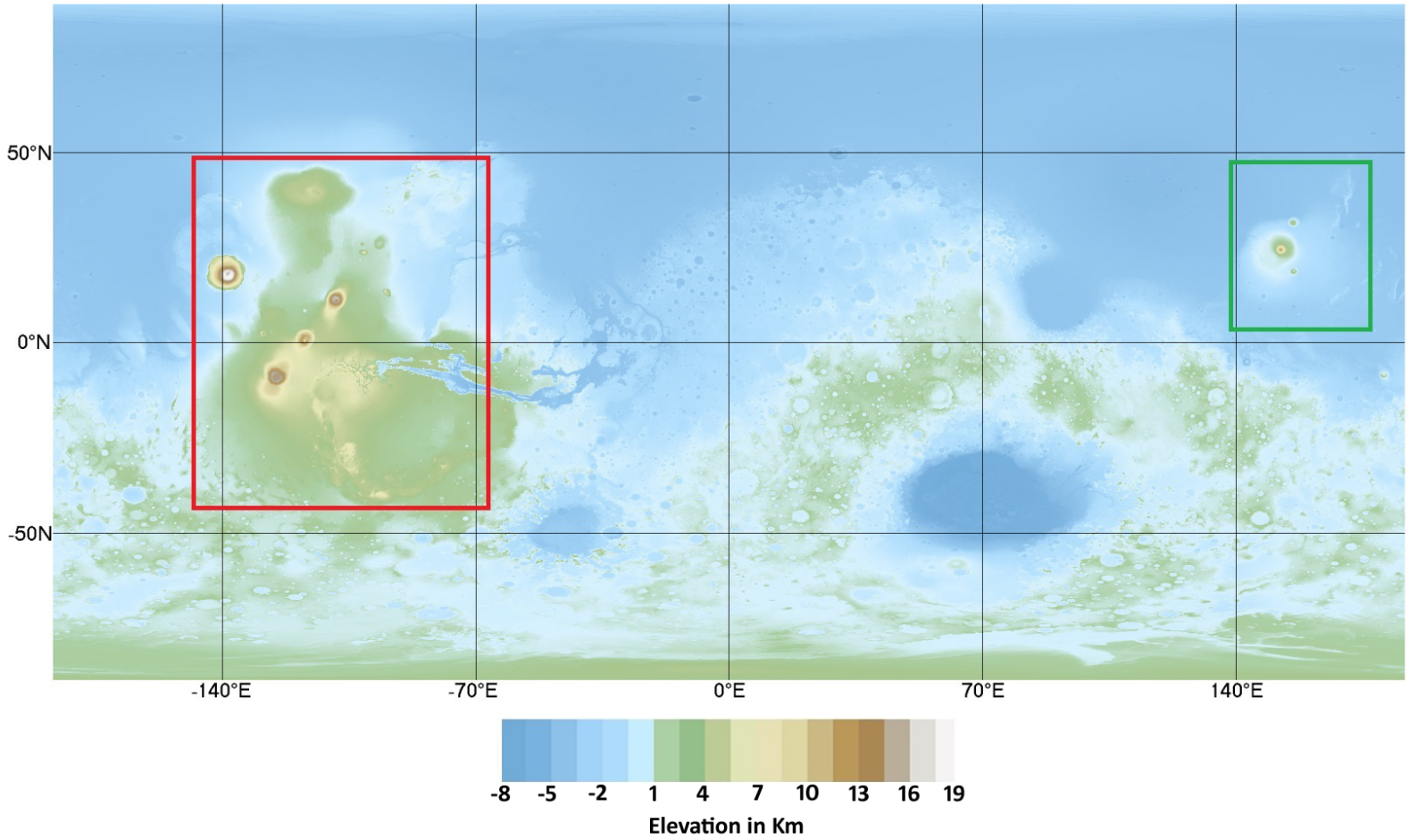

Figure 1.2 Global elevation map of Mars using Mars Orbiter Laser Altimeter (MOLA) data. The red and green squares represent the Tharsis and Elysium regions, respectively.

1.5 Important morphological features in lava region

Apart from the volcanic shields and plains, several other important morphological features are exhibited in the volcanic regions of Mars. These features provide key information about the past geological activities that have shaped the Red Planet Mars. A few of them are discussed here:

1.5.1 Grabens:

Numerous grabens extend radially away from the Tharsis Montes (Wise et al., 1979a, 1979b; Plescia and Saunders, 1982; Wilson and Head, 2002), and they extend in the range of a few hundred meters to thousands of kilometers (Figure 1.3). Geological maps and crater counting confirm their persistence throughout the Noachian to Amazonian periods (Scott and Tanaka, 1986; Tanaka et al., 1992; Tanaka et al., 2014), yet the formation process is still elusive. Two hypotheses emerged from the earlier studies in the formation process of these graben systems: i) tectonic process (crustal extension) only (Plescia and Saunders, 1982; Banerdt, W.B. et al., 1992; Phillips, R.J. et al., 2001) ii) magmatic and tectonic processes (where extension and dikes both are involved) (Mège, D., and Masson, P., 1996; Ernst, R.E. et al., 2001; Wilson, L., and Head, J.W., 2002; Scott et al., 2002; Mège, D. et al.2003).

The first hypothesis emerged from large scale volcanism and extensive fracturing resulting from the loading of the lithosphere by voluminous extrusive and intrusive magmatic deposits in the Tharsis region (Zuber, 2001; Phillips, R.J. et al., 2001). The second hypothesis involves the underlying dike injection and dike swarms in the grabens formation process

(Mège and Masson, 1996b; Ernst et al., 2001; Wilson and Head, 2002; Scott et al., 2002; Head et al., 2003; Mège et al., 2003; Schultz et al., 2004). A model study suggests that the forcible widening by dikes alone is not sufficient to produce a graben at the surface (Wyrick and Smart, 2009). But, another study by Schultz et al., 2004 conclude that the Memnonia graben system (located south of and parallel to Mangala Fossa) is most consistent with a dike-induced origin and least compatible with a faulting-based origin, but they also observed that the other Tharsis radial grabens do not consistently reveal dike-related topographic signatures. However, most of these studies used topography data or modeled the formation process using crustal mechanics and fluid dynamics.

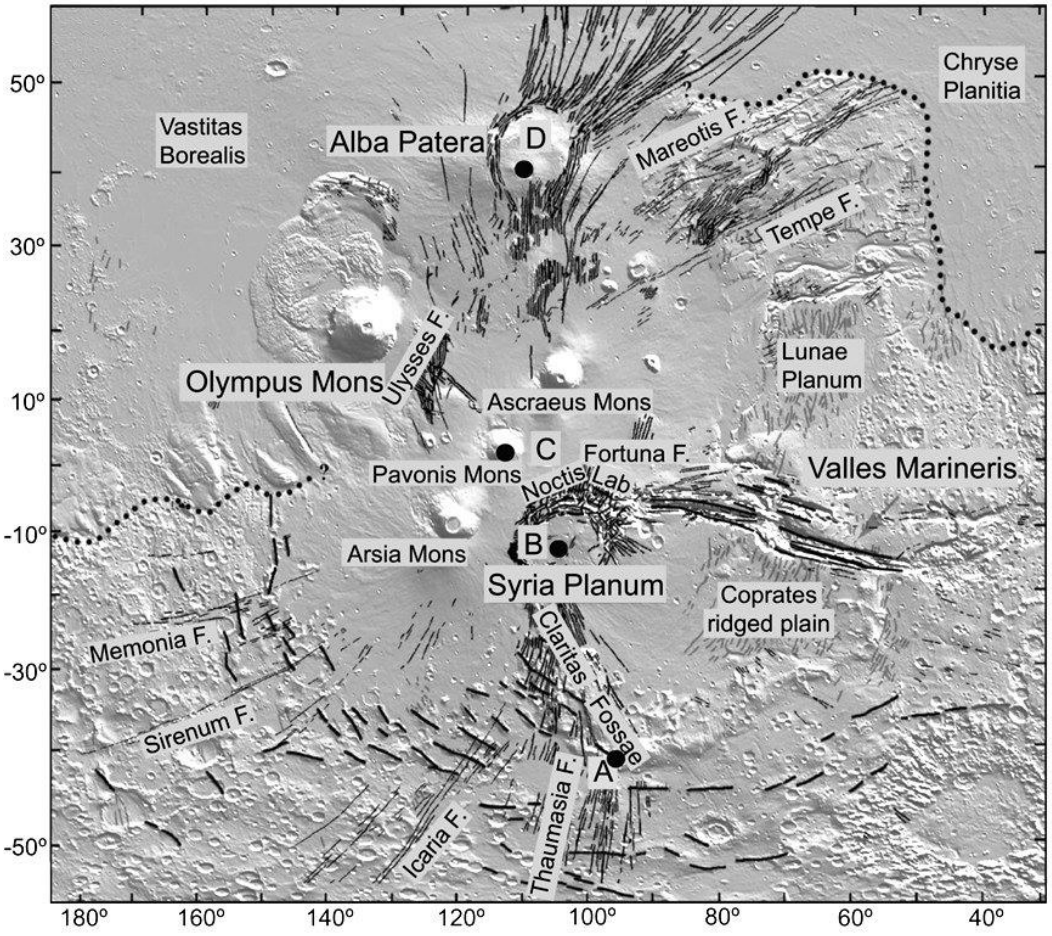

Figure 1.3 Distribution of graben systems (black line) in the Tharsis region of Mars (Source: Large Igneous Provinces, Cambridge University Press)

1.5.2 Infilled craters

Many deeply infilled craters are observed on Mars (Figure 1.4). These craters were first observed by Mariner 4 in 1965, and various processes to fill Martian craters have been proposed, including aeolian sedimentation (e.g. Arvidson, 1974, Christensen, 1983, McDowell and Hamilton, 2007), lacustrine sedimentation (e.g. Newsom et al., 1996, Cabrol and Grin, 1999, Fassett and Head, 2005, Pondrelli et al., 2005) and impact processes such as impact melt ponding or volcanism (e.g. Smrekar and Pieters, 1985, Wilhelms et al., 1987).

Numerous infilled craters of varying sizes are visibly present in the Tharsis region. Several processes may have led to the formation of the present day crater floors. Since Tharsis region formation process is mainly comprises of lava so the most likely scenario of infilling of these craters are volcanic infilling through the nearby volcanic vents like Tharsis Montes or Elysium Mons.

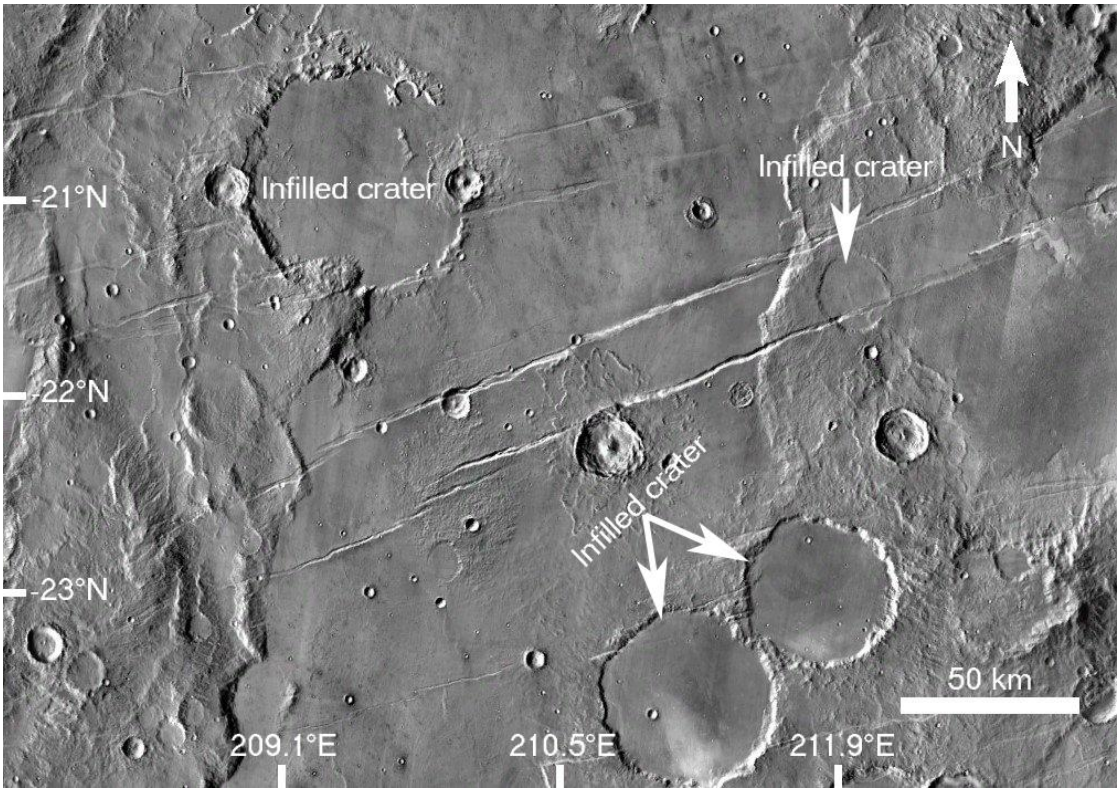

Figure 1.4 A select few infilled craters in the Tharsis region on Mars (Image: Daytime THEMIS, Mars Express)

1.5.3 Multi Layered ejecta (MLE) crater

Although impact craters have been identified on many planetary bodies, a class of craters with a specific type of ejecta known as Multi Layered Ejecta (MLE) was first identified on Mars (McCauley, 1973) (Figure 1.5). The formation hypothesis is that the energy of an impactor causes sub-surface ice to become fluid and flow outward. The MLE craters are identified by their ejecta deposits, which are the material that resettles around a crater following an impact (Hoover et al., 2021). Such craters give an idea about the location of the presence of subsurface ice.

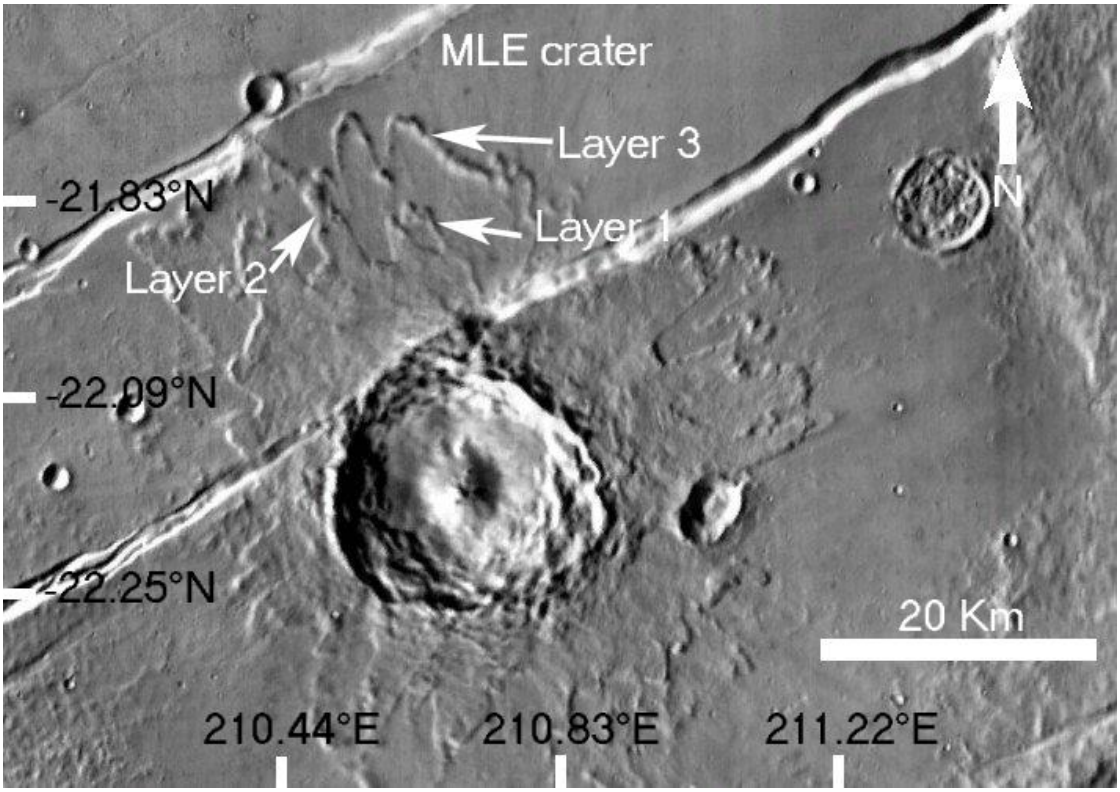

Figure 1.5 Multi Layered Ejecta (MLE) crater in the Tharsis region on Mars (Image: Daytime THEMIS, Mars Express)

1.5.4 Outflow channels

Outflow channels are marked as large depressions on Mars up to tens of km wide, hundreds of km long, and up to a km deep (McCauley et al. 1972; Carr and Clow ,1981; Baker et al. 1992). They may commence abruptly in collapsed and disrupted chaotic terrains at full width, are deepest at the head, and decrease in size distally (Sharp and Malin, 1975). Few major outflow channels, like Mangla Vallis (Figure 1.6), Kesai Vallis, and Athabasca Vallis, are located in the lava region. These outflow channels are an indicator of fluvial activities in these regions.

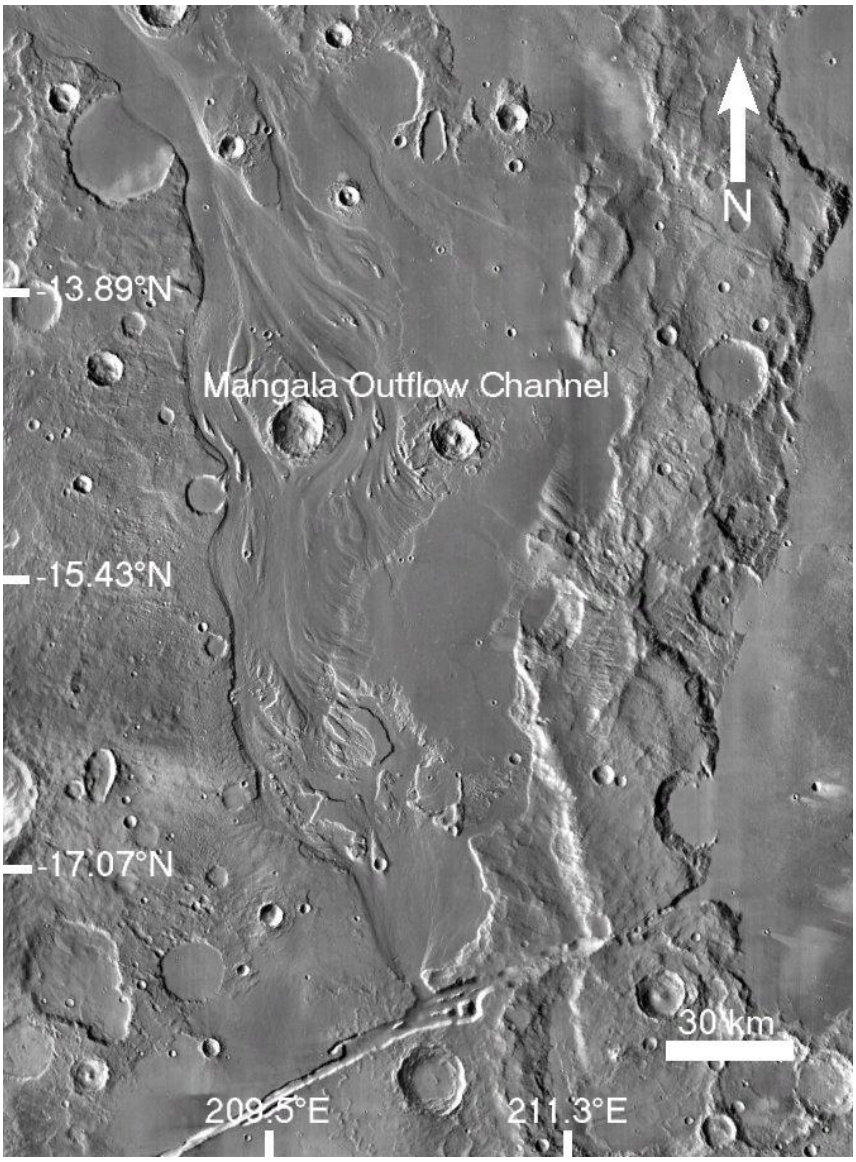

Figure 1.6 Mangala Vallis outflow channel in the Tharsis region on Mars (Image: Daytime THEMIS, Mars Express)

The above morphological features indicate that the lava region on Mars is diversified and geologically very active. The lava covered the entire region, and many geological features were hidden beneath it. These submerged features are very important in understanding the past geological activities. Most of the understanding of past geological activities

is only through morphological studies. To overcome these limitations, the European Space Agency (ESA) and the National Aeronautics and Space Administration (NASA) sent two radar systems to investigate the Martian subsurface, namely Mars Advanced Radar for Subsurface and Ionosphere Sounding (MARSIS) and SHAllow RADar (SHARAD).

MARSIS onboard Mars Express, the first European interplanetary mission, was launched in 2003 and started the investigation of the Martian subsurface in July 2005. The primary goal of these subsurface radars was to search for ice and water in the Martian subsurface (Orosei et al., 2015). For the first time MARSIS observed the internal structure of Planum Boreum outlining the Basal Unit, an icy deposit lying beneath the North Polar Layered Deposits (Byrne, 2009). It also observed radar properties of the subsurface unit in the Vastitas Borealis, which indicates large quantities of ice buried beneath the surface (Mouginot et al., 2012). Despite the major achievements, the low operating frequency (1.3-5.5 MHz) and higher wavelength of 230 meters in free air, the resolution of MARSIS was poor and did not resolve the upper layer of the subsurface unit.

Considering the above limitations, the Italian Space Agency provided a higher frequency radar, SHARAD, as a facility instrument onboard the NASA mission Mars Reconnaissance Orbiter (MRO) in 2005 (Seu et al., 2005,2007). With 20 MHz central frequency and 15 meters wavelength in free air, SHARAD started the primary science phase in October 2006. In its 16 years of operation, it covered more than 55% of the Martian surface with 32800 discrete orbit segments (Putzig et al., 2023). The primary science objective of the SHARAD experiment was to map, in selected locales,

dielectric interfaces to several hundred meters depth in the Martian subsurface and to interpret these results in terms of the occurrence and distribution of expected materials, including competent rock, regolith, water and ice, with a vertical resolution of ~10 m and a horizontal resolution of a few hundred meters (300 m – 1 km). During its operation, SHARAD's remarkable achievements like the revelation of the construction, composition, and history of North Polar Layer Deposit (NPLD) (Phillips et al., 2008; Putzig et al., 2009), uncovered the mid-latitude glacial landforms are ice-rich debris-covered glaciers (Holt et al., 2008; Plaut et al., 2009) and constraints on the interior composition and stratigraphy of volcanic and sedimentary layers (Carter et al., 2009a; Shoemaker et al., 2022; Simon et al., 2014, Bharti et al., 2021).

The above findings confirmed that the SHARAD is capable of investigating the subsurface for every type of geological unit. Using this ability, SHARAD data has been used with other data sets to study the Martian lava region to find new geophysical evidence and its formation process, which is still unreported.

Presently, the Tharsis region is covered with lava, but as mentioned above, two features, infilled craters and graben systems, are dominant morphological features in this region. My focus of the study is on understanding the formation mechanism of these two important geomorphological features via geophysical evidences to further upon the current understanding.

1.6 Research Motivation

As mentioned above, infilled craters and graben systems are prominent geomorphological features in the volcanic regions of Mars, particularly in the Tharsis belt. Many hypotheses are given to explain the formation of these two geological features, but no general agreement has been reached so far. These hypotheses are discussed in detail in Chapters 4 and 5. In this thesis, subsurface radar data and a three-layer model have been used for the first time to understand the infilling process (Chapter 4). Dielectric constant of the infilled material has been estimated for Lal crater in the Mangala area. My other study (Chapter 5) deals with the graben systems and tries to constrain the formation process. These two studies help us to understand the role of these geological processes during the evolution of Mars.

1.7 Objectives

The following are the specific research objectives of my thesis work, which is broadly aimed towards enhancing our understanding of the evolution of Tharsis, the major volcanic region on Mars.

(i) To find out geophysical evidence for other geological processes in the lava covered Tharsis region.

(ii) Surface and subsurface investigation of graben systems to decipher the formation process. Whether tectonic only or tectonic and magmatic, both processes are involved?

(iii) To prepare a multilayer model to decipher the dielectric properties of subsurface material. This model is useful for deciphering the dielectric

properties of the subsurface material in the volcanic regions of Mars. This model can also be used in other regions of Mars to find out the dielectric properties of buried materials.

1.8 Outline of the Thesis

The remainder of this Thesis leads through a discussion of our current understanding and new research on volcanic regions of Mars. Each chapter stand on its own, however, they include references to sections in other chapters. A brief description of the subsequent chapters is as follows:

Chapter 2: Data, Tools and Methodology

This chapter includes a detailed description of the datasets utilized in this thesis work and their sources. SHARAD data is the major dataset utilized in this work, so a detailed discussion has been provided about SHARAD and its data processing. This chapter also discusses the GIS tools used. A flowchart has been included to understand the methodology, which includes the different steps undergone to reach the conclusions.

Chapter 3: Subsurface Dielectric Constant: Concept & Modeling

In the radar study, estimating the subsurface material property is very important. Chapter 3 discusses in detail the conceptualization of a three-layer model to estimate the dielectric constant of subsurface material.

Chapter 4: Nature of Infilling in the Lal crater

The chapter starts with an introduction, including the primary objective of the study which includes (i) a discussion about the study area, (ii) morphology and geophysical study of the study area, (iii) SHARAD observation, (iv) model discussion, (v) infilling hypothesis, and (vi) result.

Chapter 5: Subsurface study of the Tharsis graben system

This chapter includes the primary objective of understanding the formation process of Martian graben systems in the lava region. This chapter contains (i) an introduction to the Martian graben system and present understanding, (ii) SHARAD observation and reflection map, (iii) constraint the electrical properties of the subsurface material, (iv) morphology and geophysical studies and scenario of subsurface deposition, and (v) result.

Chapter 6: Summary and Future Prospects

The overall summary and conclusions of the research work is provided in this chapter. An emphasis has been made upon the future prospects of the use of subsurface radar system for Martian geology.

Chapter 2

Data, Tools, and Methodology

The primary data used in this thesis are shallow radar, visible imagery, and DEM. The technical details of these remote sensing datasets and their processing methodology are provided as follows:

2.1 SHAllow RADar (SHARAD)

2.1.1 About SHARAD

SHARAD is a 10m wide dipole antenna onboard NASA's Mars Reconnaissance Orbiter that operates with a 20 MHz center frequency and 10 MHz bandwidth (Seu et al., 2004, 2007) (Figure 2.1). The signal provides a 15 m vertical resolution in free space that improves to ($15/\varepsilon^{1/2}$) meters in a medium of relative permittivity ε (Seu et al., 2004, 2007). The horizontal surface resolution is based on the Fresnel zone of the signal that reaches the surface, i.e., 3-6 km. This can be improve the along-track direction by data processing to 0.3–1 km (Seu et al., 2004, 2007). Radar waves that reach the surface are reflected in part, and some signal penetrates into the sub-surface, where it produces reflections if they reach a contrast sufficiently large in permittivity of the upper and lower materials.

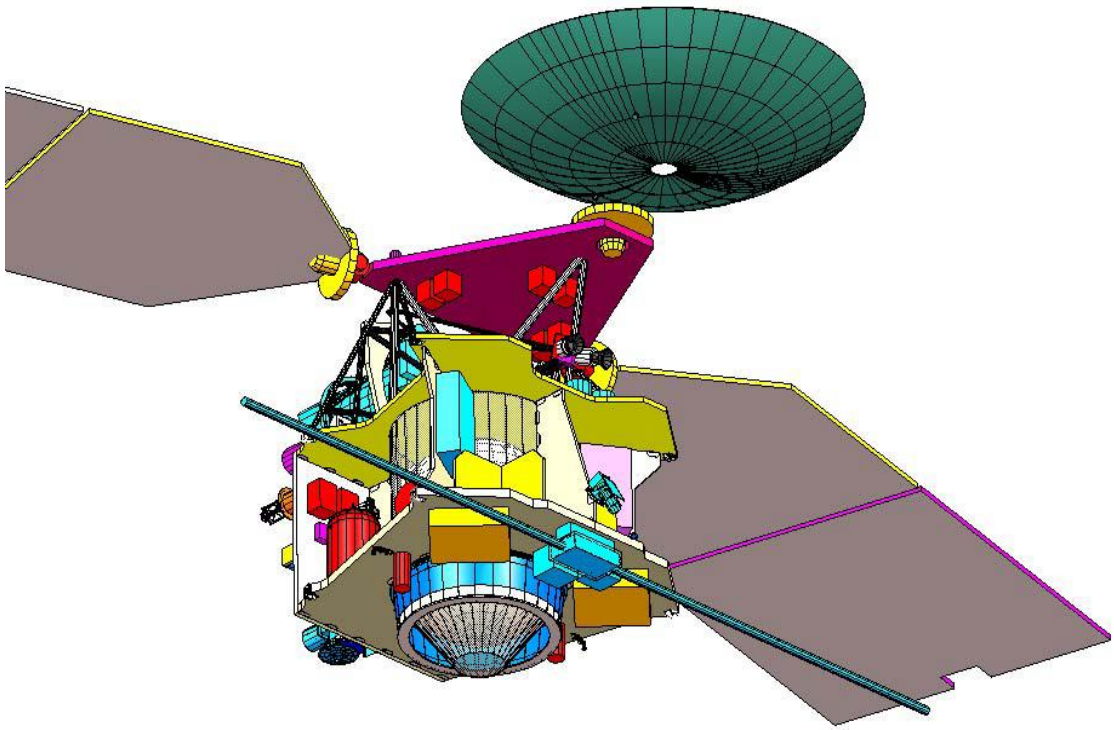

Figure 2.1 Mars Reconnaissance Orbiter spacecraft with SHARAD dipole antenna (Image Courtesy: NASA).

2.1.2 SHARAD data Analysis

Surface returns may come from directly below the spacecraft (nadir) or off to the side (off-nadir), out to several km. Both types of reflections are measured in time delay, and the undesirable off-nadir reflections may arrive simultaneously or later than desired signals from the nadir, confusing the interpretation of the subsurface signal. These off-nadir returns are commonly referred to as surface "clutter." To identify and mitigate the effects of clutter, simulated radargrams (Choudhary et al., 2016) have been used. MOLA gridded topography data is used to generate the simulated radargram (Smith et al., 2001). Reflections that occur in the observed radargram but not in the simulated radargram are interpreted as subsurface interfaces that can be studied (Figure 2.2). With this approach, one can distinguish between the radar signal of the surface and the subsurface. A detailed description of the clutter mitigation can be found in Smith and Holt, 2015. In this thesis, Reduced Data Records (RDR) have been used to analyze the SHARAD radargram, which is processed by the U.S. members of the SHARAD team and is publicly available at the Planetary Data System (PDS) node: https://ode.rsl.wustl.edu/mars/datasets. These data are required to be converted into an industry-standard seismic data format (.segy) for further processing. For this purpose, the Colorado SHARAD Processing System (CO-SHARPS, Putzig et al., 2016) has been used. Subsequently commercially available geoscience software is needed to interpret these converted .segy data. In this study, SeisWare™ has been used to interpret the .segy data and map the extent of distribution of the subsurface reflections.

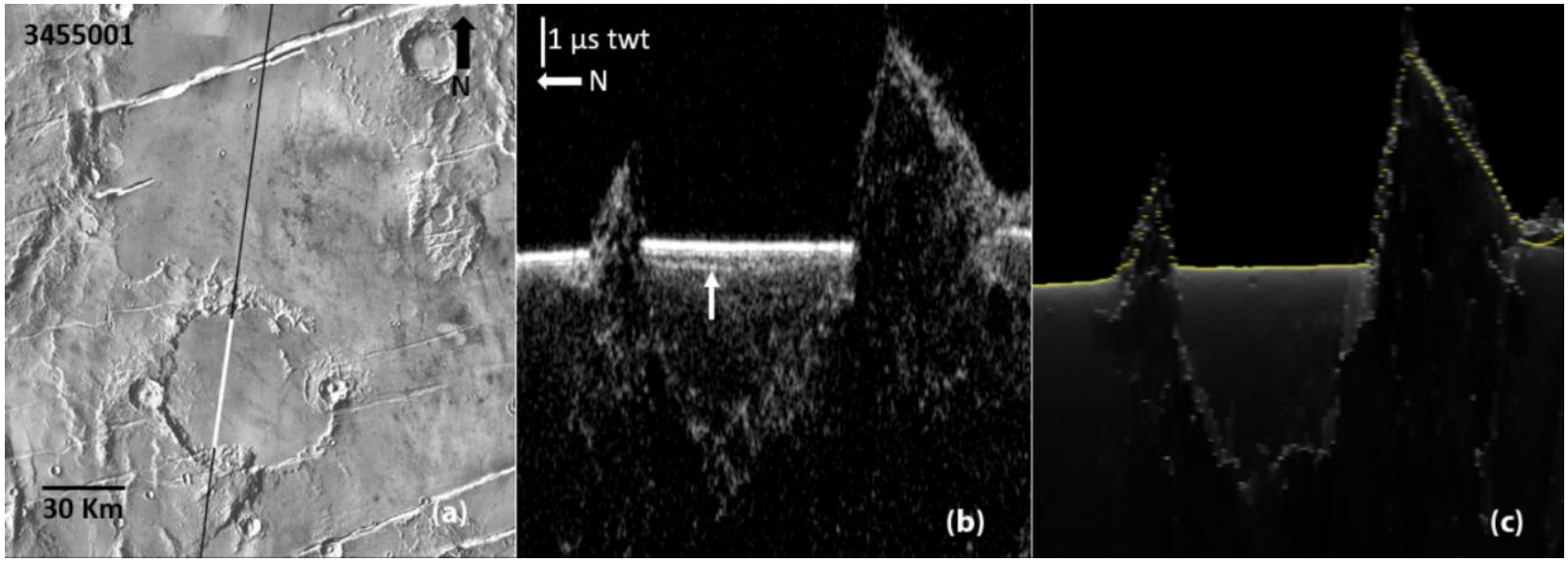

Figure 2.2 Subsurface reflections at Lal crater: *a)* the daytime THEMIS images with the SHARAD ground tracks 3455001. The white patch indicates the extent of a subsurface detection in (*b*). *b*) SHARAD radargrams 3455001 shown in two way time (twt) delay; the vertical white arrow indicates the subsurface reflection. *c)* Simulated radargrams displaying off-nadir topographical clutter echoes. No clutter is found inside the crater, so the reflector is interpreted to indicate a subsurface interface.

After comparing the radargram signals to the simulated "cluttergrams" (Figures 2.2 c), subsurface reflections and interfaces between different dielectric materials at the crater (arrows in Figure 2.2 b) can be identified. Numerous SHARAD radargrams were investigated over the Lal crater, Mangala Fossa and Labeatis Fossa and those observations in which clutter is not apparent and sufficient contrast is present to demonstrate subsurface reflections were identified**.**

2.2 Digital Elevation Model (DEM) and Imagery Data

Digital Elevation data is used to project the topography of the study area. For this purpose, the Mars Orbiter Laser Altimeter (MOLA) and blended version of MOLA and High-Resolution Stereo Camera (HRSC) are used in this study. The blended version is generated by utilizing the ~463 m/pixel MOLA DEM and blending it with the HRSC DEMs (~50 m/pixel) into it (Fergason et al., 2018). The final blended MOLA-HRSC DEM has a spatial resolution of ~200 m/pixel (Fergason et al., 2018). MOLA data can be accessed through the following link: Planetary Data System (PDS) PDS Geosciences Node Data and Services: MGS MOLA (wustl.edu) and MOLA-HRSC DEM can be from http://bit.ly/HRSC_MOLA_Blend_v0 .

Imagery data have been used to investigate and display the local morphological features and SHARAD track. The MRO Context Camera (CTX), MOM Mars Color Camera (MCC) and Mars Odyssey Thermal Emission Imaging System (THEMIS) data are used in this study. CTX has a spatial resolution of 6m/pixel, and resolution of THEMIS is 18m/pixel. MCC onboard MOM has been used for global depiction of Mars.

Table 2.1 Summary of instruments and datasets used in this thesis

Spacecraft	Space Agency	Instrument	Data Type	Wavelength	Resolution	Uses
Mars Reconnaissance Orbiter	NASA	SHARAD (Provided by Italian Space Agency)	Radargram	15 m in free space	Along track: 0.3–1 km Cross track: 3–6 km	Observe the dielectric discontinuity in the subsurface
Mars Reconnaissance Orbiter	NASA	CTX	Imagery	500 to 800 nm	~6 m/pixel	Investigate the local features
Odyssey	NASA	THEMIS	Imagery		18 m/pixel	Map the SHARAD radargram.
Mars Global Surveyor (MGS)	NASA	MOLA	DEM		300 m/pixel	Topography map
Mars Orbiter Mission	ISRO	MCC	Imagery		19.5 m/pixel	Global image

2.3 GIS Tools used

ENVI, ArcGIS, QGIS, CO-SHARPS, JMARS, and SeisWare® are used as GIS software tools to interpret the data. PRL has a license version of ENVI (The environment for visualizing Images) and ArcGIS. QGIS is an open-source GIS software package.

Colorado SHARAD Processing System (CO-SHARPS) is an online processing boutique. This is jointly developed by Jet Propulsion Laboratory (JPL), Smithsonian National Air Space Museum, and Jackson School of Geosciences and hosted by Planetary Science Institute, Colorado, USA, and Tucson, Arizona, USA. Using this boutique, the radargram can be simulated to distinguish the clutter and subsurface reflection, generate .sgy (Seismic Expert Group) data to display the data in time series, and convert the radargram into depthgram. Access to this boutique is on request only.

JMARS is an acronym that stands for Java Mission-planning and Analysis for Remote Sensing. It is a geospatial information system (GIS) developed by ASU's Mars Space Flight Facility, Arizona State University, to provide mission planning and data-analysis tools to NASA scientists, instrument team members, students of all ages, and the general public. JMARS has multiple mission data, and these data can be displayed in layers. This application has been used to study the topography around the reflection area by generating high resolution maps.

SeisWare® is a Geophysical Software. It is used to analyze the SHARAD data. SeisWare® is very generous in distributing academic licenses to academic institutions. PRL also has an academic license of this software.

2.4 Methodology

As mentioned earlier, the present-day Tharsis region is covered with lava. So, subsurface shallow radar is a useful instrument for looking beneath the surface. The study area was chosen based on earlier studies and geomorphological features. Then, the methodology mentioned in Figure 2.3 is followed to reach the final scientific conclusion.

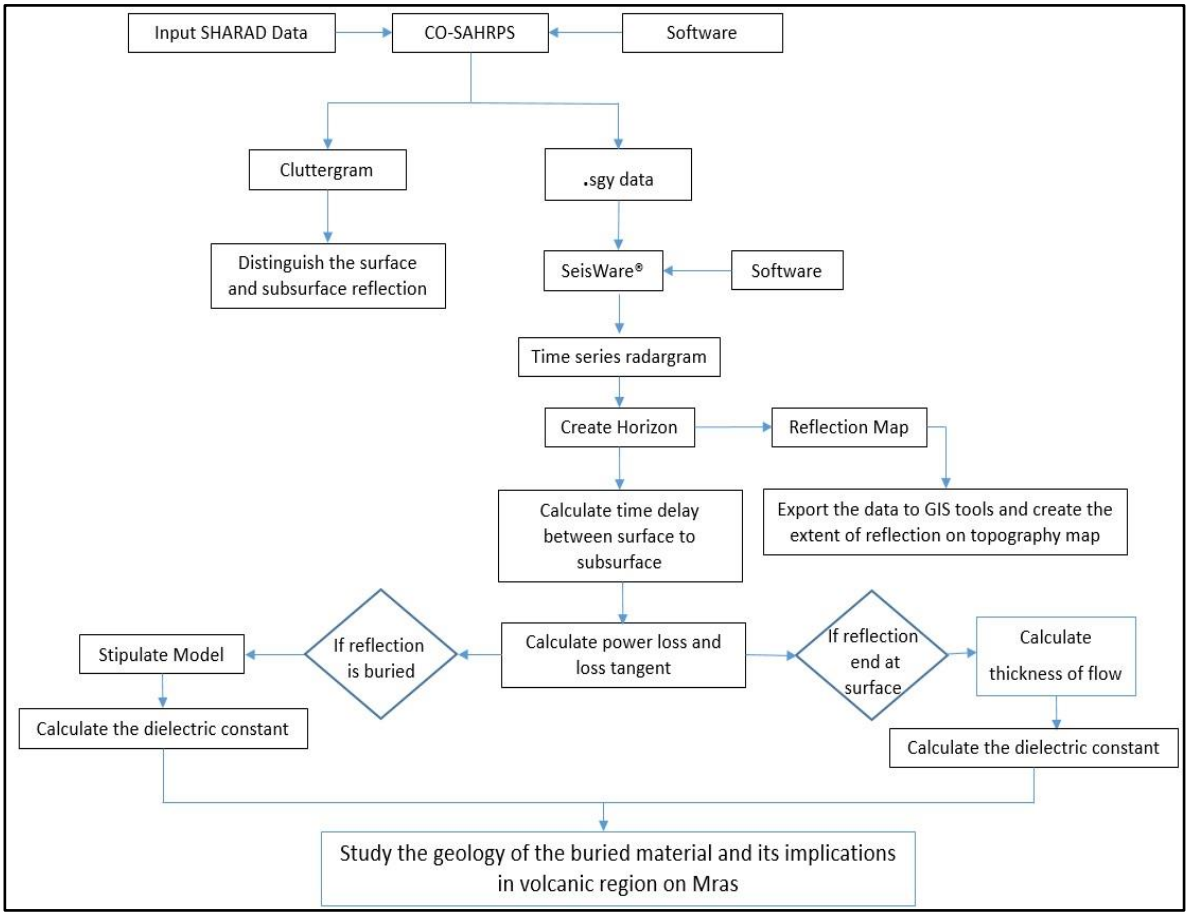

Figure 2.3 A schematic flowchart depicting the basic methodology adopted to address the objective of the thesis.

Chapter 3

Subsurface Dielectric Constant: Concept & Modeling

Mars is a morphologically diversified planet. This diversification requires development of different scientific approaches to study the planet. Any given approach for one location may or may not be applicable for other locations. Hence, multiple approaches and validation are needed to reach any scientific conclusion. In this Thesis, the study area is a major lava region, i.e., Tharsis, and the aim is to identify the buried material. This induces a new dimension to look at the lava region. This also demonstrates the capability of radar to decipher the new scientific objective.

One of the most important aspects of radar study is to find out the dielectric properties of the buried material. Two types of topography of the buried material are observed. One is completely buried, and the second is lava flow visible on the surface. In both the conditions, different methods are used to estimate the dielectric properties of the buried material. In the Lal crater, the subsurface material is completely buried, hence, an appropriate model is needed to estimate its dielectric permittivity. In this context, a three-layer model is conceptualized - A schematic of the physical model is presented in Figure 3.1.

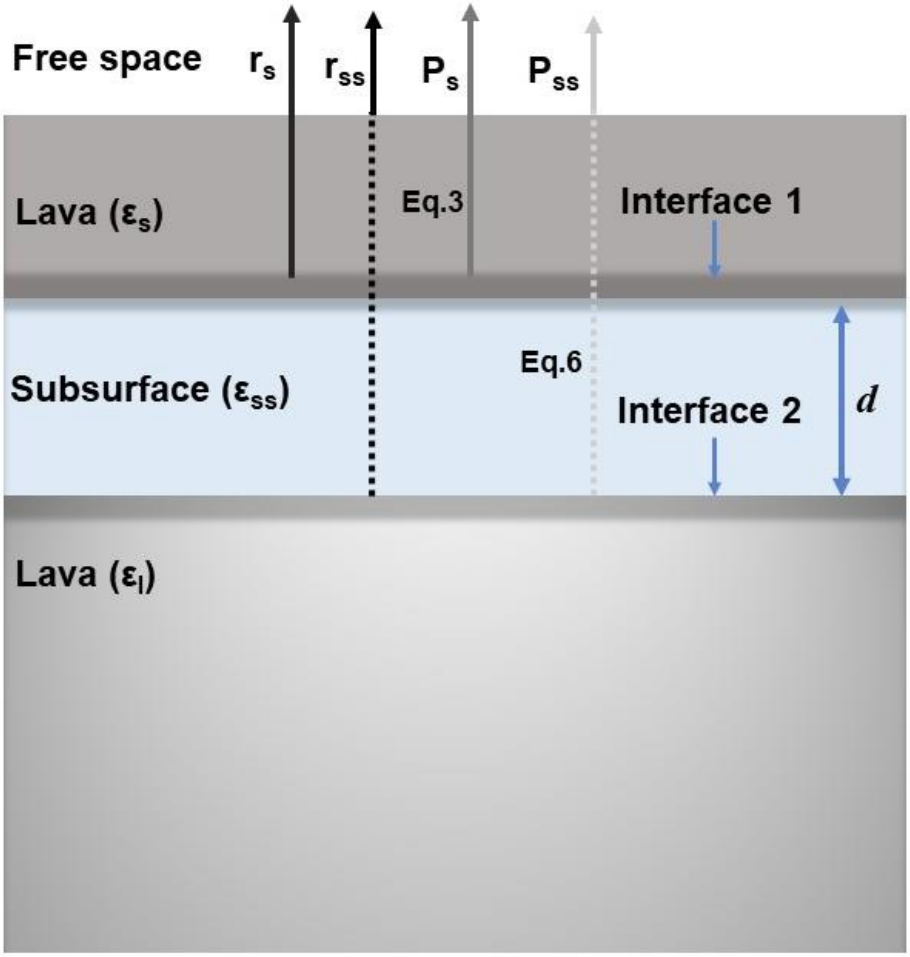

Figure 3.1 Schematic of the physical model used in our calculations. The subsurface layer (ε_{ss}) is sandwiched between the top (ε_s) and bottom (ε_l) units that are assumed to be composed of lava. The plane joining the ε_s and ε_{ss} is Interface 1, and ε_{ss} and ε_l are represented at Interface 2. r_s corresponds to the coefficient of reflection due to top unit (ε_s), while r_{ss} infers the reflection coefficient appeared at Interface 2. P_s and P_{ss} refer to the respective signal powers received by the receiver after reflection from top lava unit (corresponding to r_s), and after reflection from subsurface layers, including the ε_l, ε_{ss}, and ε_s (*corresponding to* r_{ss}) – the measured P_s and P_{ss} are supplied into Eq. (3) and Eq. (6), respectively.

This model has assumed that the present surface at the reflection site (top most unit) is composed of a thin lava unit. The assumption is based on the observation of numerous meter-scale ghost craters on the surface of the Lal crater. These craters have an average diameter in the range of ~30 to 50 m. Using the d/D ratios of 0.03 (McEwen et al., 2005), the depth of these craters varies in the range of ~1.19 to 2.8 m. The geologic observations (Tanaka et al., 2014) and the derived depth values indicate that the uppermost layer is a thin lava unit. The buried material is considered as "the subsurface layer (ε_{ss})", i.e., sandwiched between two geological units, i.e., the top unit (ε_s) and the bottom unit (ε_l). In the later section, it is depict that the uppermost layer is thinner than the vertical resolution of SHARAD, where the methodology of Alberti et al., 2012; Morgan et al., 2015; Lalich et al., 2019 is adapted to handle thin layer calculations. Using this methodology, the first bright reflection may be considered to emerge from the combined effect of two reflections at the air-lava interface and the lava-subsurface interface (Interface 1). In model it is assigned an effective permittivity of ε_s. Below the subsurface layer in question, the bottom unit (ε_l) is assumed to be composed of lava.

The reflection from the bright top interface may be characterized by Fresnel reflection (Alberti et al., 2012). Now, the transmitted wave signal through this top layer acts as an incident signal for the subsurface (ε_{ss}) and bottom lava unit (ε_l). The coefficient of reflection for combined units of ε_{ss} and ε_l is calculated using the linear theory of electromagnetic (*em*) wave propagation having linear (*s*) polarization and normal incidence, that may be characterized by the wave equation $\nabla^2 E + k_o^2 \varepsilon E = 0$ (Gurevich, 1978),

where E is the electric field amplitude, and ε is the dielectric constant of the medium. After the information of the reflection coefficient of the subsurface layer (ε_{ss}), this estimate is combined with the top layer (ε_s) reflectance (using Fresnel relation of inversion) to calculate the effective reflection coefficient for a three-layered model setup.

Following Fresnel's formulation, the reflection power (P_s, bright reflection) and the power transmitted (P_T) through the top layer (ε_s) may be given in terms of incident power (P_i) as,

$$P_s = r_s^2 P_i \tag{3}$$

$$P_T = (1 - r_s^2) P_i, \tag{4}$$

where $r_s = (k_o - k_s)/(k_o + k_s) = (1 - \varepsilon_s^{1/2})/(1 + \varepsilon_s^{1/2})$ refers to the reflection coefficient from the top lava layer (ε_s).$k_s = k_o\varepsilon_s^{1/2}$, $k_o = (2\pi v/c)$, k_s and ε_s are the wavenumbers and real part of the dielectric constant associated with the top lava layer, and v is the mean operating frequency of SHARAD.

The power (P_T) transmitted through the top lava layer (ε_s) acts as an incident power for the subsurface layer (ε_{ss}). Following the theory of linear wave propagation through a lossless medium (i.e., ε_{ss}), and matching the continuity of the wave solutions and their derivatives at both the subsequent interfaces (1 and 2), the optimum value of reflection coefficient at interface 1 may be represented as

$$r_1 = (k_s k_l - k_{ss}^2)/(k_s k_l + k_{ss}^2) = (\varepsilon_s^{1/2}\varepsilon_l^{1/2} - \varepsilon_{ss})/(\varepsilon_s^{1/2}\varepsilon_l^{1/2} + \varepsilon_{ss}), \tag{5}$$

where $k_{ss} = k_o\varepsilon_{ss}^{1/2}$ and $k_l = k_o\varepsilon_l^{1/2}$ are the wavenumbers associated with the subsurface layer (ε_{ss}) of the unknown thickness or dielectric properties and a bottom unit (ε_l) that was assumed as lava. It should be noted here that Eq. (5) yields a physically consistent solution only when $\varepsilon_{ss} < (\varepsilon_l\varepsilon_s)^{1/2}$, i.e.,

$r_1 > 0$. This approach of linear *em* (electromagnetic) theory is a standard method to calculate the reflection and transmission coefficient of the propagating wave through the medium and was recently applied by Courville et al. (2021) to examine the reflection from a multilayer deposit of NPLD (North Pole Layer Deposit).

Eq. (5) refers to the combined effects of the wave reflection coefficient (amplitude) to the subsurface (ε_{ss}) and bottom lava unit (ε_l). The power reflected at the boundary of ε_s and ε_{ss} (Interface 1) can thus be expressed as $P_1 = r_1^2 P_T = (1 - r_s^2) r^2 P_i$. This power then transmits through the top layer (ε_s) and then propagates through the free space to reach the receiver. The net power returned to the receiver can be obtained using Fresnel's formulation for transmission (similar to that used in obtaining Eq. (4)). Following this, and substituting our values, the net power reaching the receiver after the subsurface (ε_{ss}) reflection may be expressed as

$$P_{ss} = (1 - r_s^2) P_1 = (1 - r_s^2) r_1^2 P_T = (1 - r_s^2)^2 r_1^2 P_i , \quad (6)$$

where the effective coefficient of reflection is $r_{ss} = (P_{ss}/P_i)^{1/2} = (1 - r_s^2) r_1$. Using Eq. (3) and Eq. (5), the ratio of the reflected powers can thus be written as

$$(P_{ss} / P_s) = (1 - r_s^2)^2 (r_1^2 / r_s^2) \quad (7)$$

Here SHARAD observations are used to measure this power ratio (P_{ss}/P_s) along the track (Table 1). With the measured value of (P_{ss} / P_s) and assumed dielectric constants of the top (ε_s) and basal unit (ε_l), Eq. (7) is used to determine the subsurface dielectric constant (ε_{ss}) (Figure 3.1). Considering Eq. (5), only those solutions have been chosen for ε_{ss} which are consistent

with $\varepsilon_{ss} < (\varepsilon_l \varepsilon_s)^{1/2}$, under this condition, Eq. (7) yields a unique solution for ε_{ss}.

Chapter 4

Nature of Infilling in the Lal crater

4.1 Introduction

The first Shallow Radar (SHARAD) based observations of the subsurface reflections within Lal crater (diameter ~65 km; centered at 21.0° S, 150.6° W) is presented here. The Lal crater is situated south of the Mangala Fossa and Mangala Valles, a major fluvial outflow channel system. It is an infilled impact crater with a flat floor. The crater is located within a region with diverse geomorphic features, including graben systems that radiate from the Tharsis Montes (Figure 4.1). The crater is also associated with these radial graben systems. At least three grabens transect the crater (Figure 4.2) but the infilling material has subsequently buried them. The infilling material is expected to have come from multiple sources, including lava that entered from a 10 km long breach in the northeast rim, connecting external lava plains to the current crater floor. Two smaller and younger ~12 km wide impact craters, Mursan and Hilsa craters, are superimposed on the eastern and western flanks of the Lal crater (Figure 4.2), and their ejecta fills portions of the crater. Later volcanic flows embayed the ejecta of the Mursan crater, but the ejecta of the Hilsa crater was not fully embayed and remains visible inside the Lal crater at outcrops (Figure 4.2).

Tanaka et al. (2014) mapped the eastern part of the crater as an early Hesperian volcanic unit (eHv) composed of flood lava, and the western part is identified as an early Noachian highland unit (eNh) of volcanic, fluvial, and basin materials (Figure 4.1). A hypothesis that is tested here is belied by this stratigraphic interpretation, that the surface material of the eastern and central portions of Lal crater is composed of relatively younger lava layers that bury units of the same sedimentary material that is exposed in the west.

This study describe previously unreported subsurface reflectors within the Lal crater detected with SHARAD (Seu et al., 2004; 2007) sounding data. Radar investigation of the subsurface-layered deposits is used to provide information about their composition, density, and structure, and subsurface reflection geometry, including multiple stratified reflections and reflection strength, is used to measure the loss tangent and model the material's dielectric permittivity. Also mapped here is the extent and estimate of the infilling volume based on observed subsurface reflections. Finally, this study identifies possible mechanisms for the emplacement of these materials and constrain their physical and compositional properties.

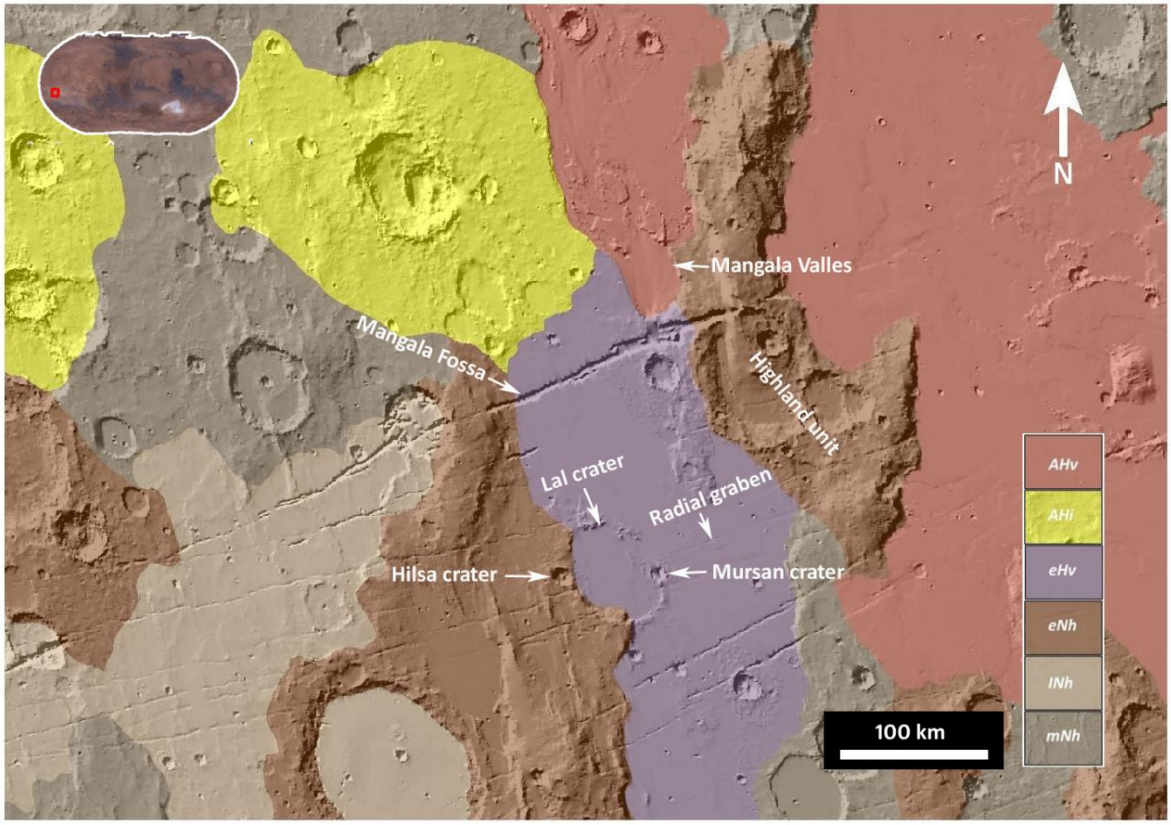

Figure 4.1 The geologic map of Mangala region (Tanaka et al., (2014)) draped over a hillshade image of MOLA 128 ppd. Here, AHv Amazonian and Hesperian volcanic unit; AHi, Amazonian and Hesperian impact unit; eHv, Early Hesperian volcanic unit; eNh, Early Noachian highland unit; lNh, Late Noachian highland unit; mNh, Middle Noachian highland unit.

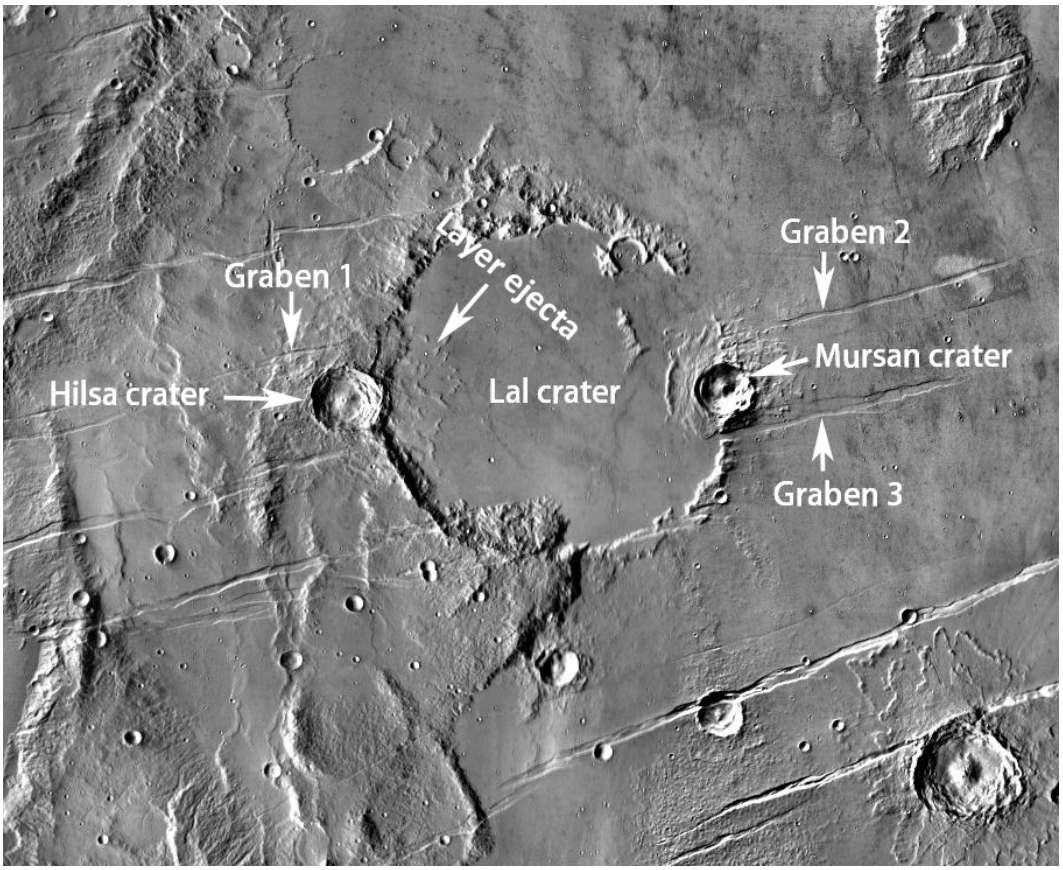

Figure 4.2 Daytime THEMIS draped over MOLA hillshade image of Lal, Hilsa and Mursan craters. Layer ejecta of Hilsa crater on the floor of Lal crater. Also three graben systems transect the Lal crater.

4.2 SHARAD Mapping of Subsurface Reflectors

Radar waves that reach the surface are reflected in part, and some signal penetrates into the sub-surface, where it produces reflections if they reach a contrast sufficiently large in permittivity of the upper and lower materials.

Surface returns may come from directly below the spacecraft (nadir) or off to the side (off-nadir), out to several km. Both types of reflections are measured in time delay, and the undesirable off-nadir reflections may arrive simultaneously or later than desired signals from nadir, confusing interpretation of the subsurface signal. These off-nadir returns are commonly referred to as surface "clutter." Here, simulated radargrams (Choudhary et al., 2016) have been generated using MOLA gridded topography data (Smith et al., 2001) to identify and mitigate the effects of clutter. Reflections that occur in the observed radargram but not in the simulated radargram are interpreted as subsurface interfaces that can be studied (Figure 4.3). With this approach, one can distinguish between the radar signal of the surface and the subsurface. A detailed description of the clutter mitigation can be found in Smith and Holt (2015). To perform the analysis, publicly available U.S. SHARAD data need to be converted into an industry-standard seismic data format (segy) using the Colorado SHARAD Processing System (CO-SHARPS, Putzig et al., 2016). Then the commercially available seismic software SeisWare™ can be used to interpret SHARAD data and map the distribution of the subsurface reflections.

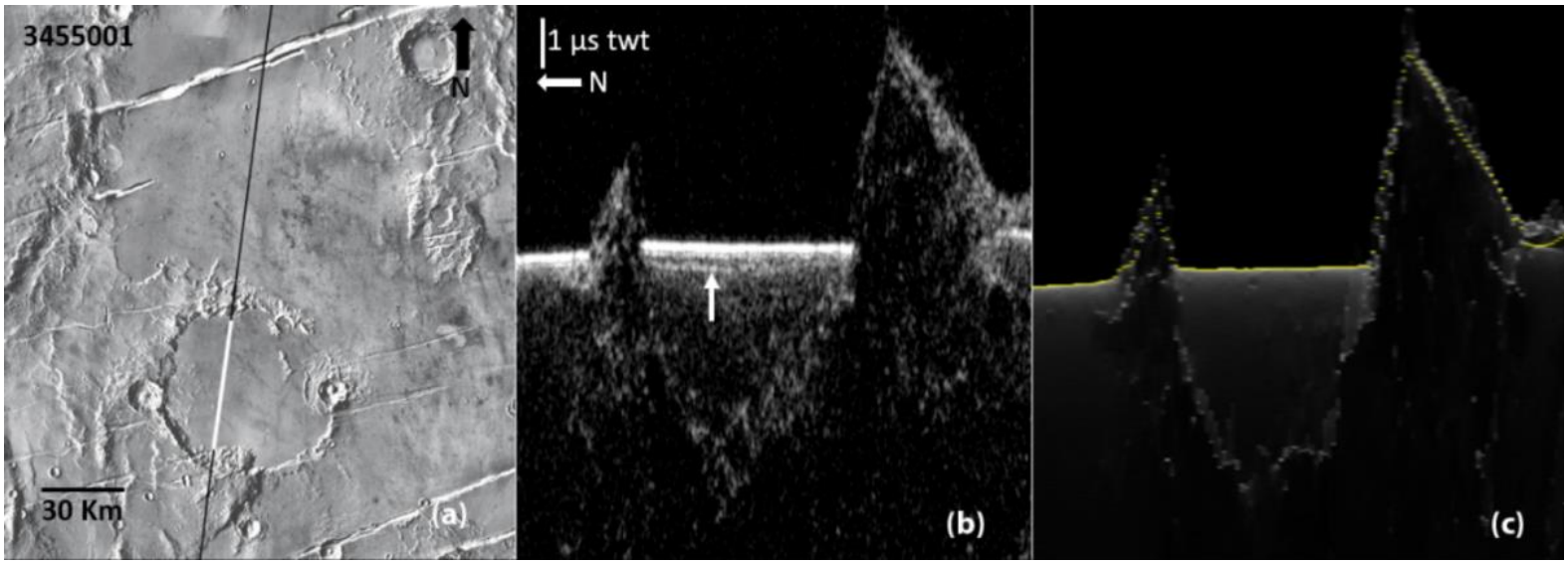

Figure 4.3 Subsurface reflections at Lal crater: *a)* the daytime THEMIS images with the SHARAD ground tracks 3455001. The white patch indicates the extent of subsurface detection in (*b*). *b*) SHARAD radargram 3455001 is shown in two-way time (twt) delay; the vertical white arrow indicates the subsurface reflection. *c)* Simulated radargrams displaying off-nadir topographical clutter echoes. No clutter is found inside the crater, so the reflector is interpreted to indicate a subsurface interface.

After comparing the radargram signals to the simulated "cluttergrams" (Figure 4.3c), it has been observed that the subsurface reflections and interfaces are present between different dielectric materials at the crater (arrows in Figure 4.3b). In this study, numerous SHARAD radargrams are investigated over the Lal crater to identify those observations in which clutter is not apparent, and sufficient contrast is present to demonstrate subsurface reflections (Figure 4.4).

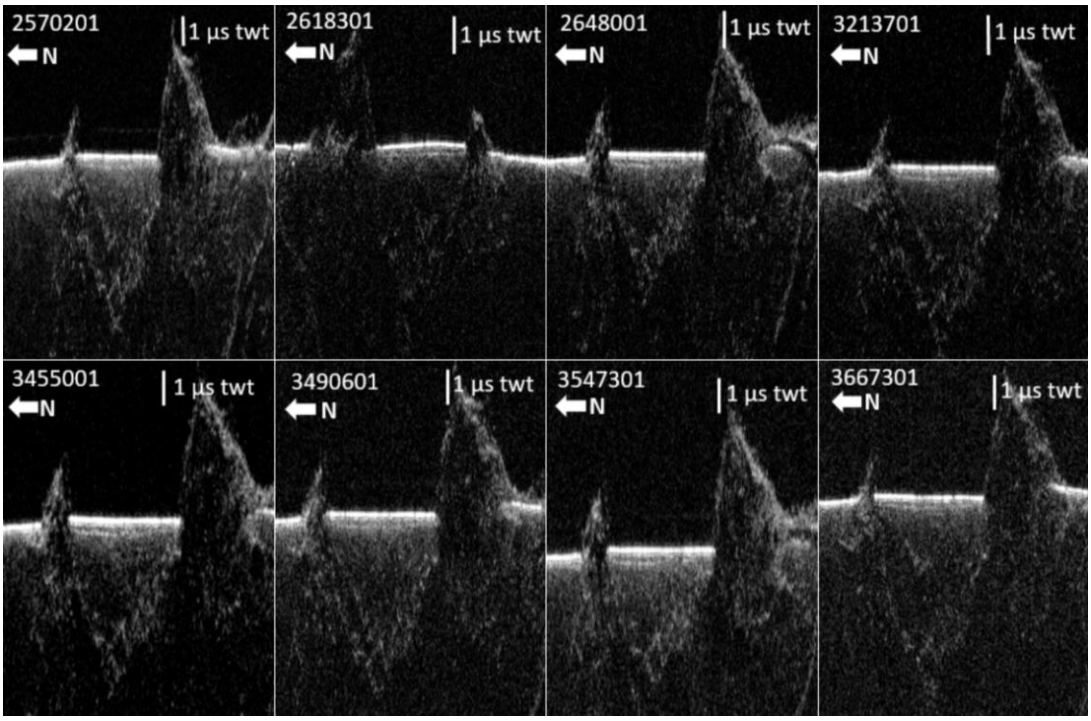

Figure 4.4 SHARAD radargrams in two-way time (twt) delay showing the subsurface reflection from the Lal crater. The SHARAD observation numbers are marked in the top left of each image.

4.2.1 Calculation of dielectric loss tangent

The loss tangent is the ratio of imaginary and real parts of the complex dielectric constant of the material, which physically represents the

power loss of the electromagnetic wave as it traverses through the medium. Along-track power of the reflectors are measured (surface and subsurface) in the SHARAD observations that cross the Lal crater to characterize the signal sensitivity in terms of the power loss (dB) and time delay (μs) (Figure 4.5). These scatter plots have been used to obtain the best possible empirical linear fit (Table 2) and determine the loss tangent of the subsurface material. The loss tangent corresponding to the subsurface dielectric interface can be expressed as,

$$tan\delta = \left[\left(2\left(\frac{\lambda}{4\pi c \Delta \tau} (lnL) \right)^2 + 1 \right)^2 - 1 \right]^{1/2} \quad (1)$$

(Campbell et al., 2008) where L is the power loss per unit of time Δτ, λ corresponds to SHARAD wavelength in free space (15 m), and c refers to the speed of light, i.e., 300 $m/\mu s$ in a vacuum.

Values of the loss tangent that are in the range of 0.008 and 0.009 (Table 2) are obtained using Eq. (1). These values are consistent with a low to moderate radar absorbing material like dry, moderate-density sediments or the lower end of the range of values measured for basalts (Campbell et al., 2008).

4.2.2 Calculation of dielectric constant

SHARAD data can be used to calculate the dielectric constant of the subsurface material with additional information such as thickness of the subsurface material and two way time delay. The measured physical values

can be constrained using the laboratory studies of terrestrial and lunar material. The permittivity (ε') can be computed from:

$$\varepsilon' = \left(\frac{c\Delta t}{2h}\right)^2 \quad (2)$$

Here, *h* is the thickness of a unit. In this case, depth of the reflecting interface from the surrounding plains as measured from MOLA topography as the thickness. Δt is the two way time delay between the top and bottom reflection as measured by SHARAD.

Subsurface interfaces within the Lal crater have no visible exposure on the surface, so it is impossible to calculate *h* directly. It leaves us with insufficient information to calculate the dielectric constant using equation 2. To remedy this, a physical model was proposed by me, in addition to the other prior constraints, to estimate a valid dielectric constant range using the SHARAD measurement. A detailed discussion about the physical model has been made in Chapter 3: "Model conceptualization to estimate the dielectric constant of the subsurface material".

4.3 Results

4.3.1 Extent of subsurface reflection

Numerous SHARAD observations that detect subsurface interfaces within the Lal crater have been found from the given SHARAD data sets. Figure 4.5 illustrates the locations and power of subsurface reflections of these interfaces.

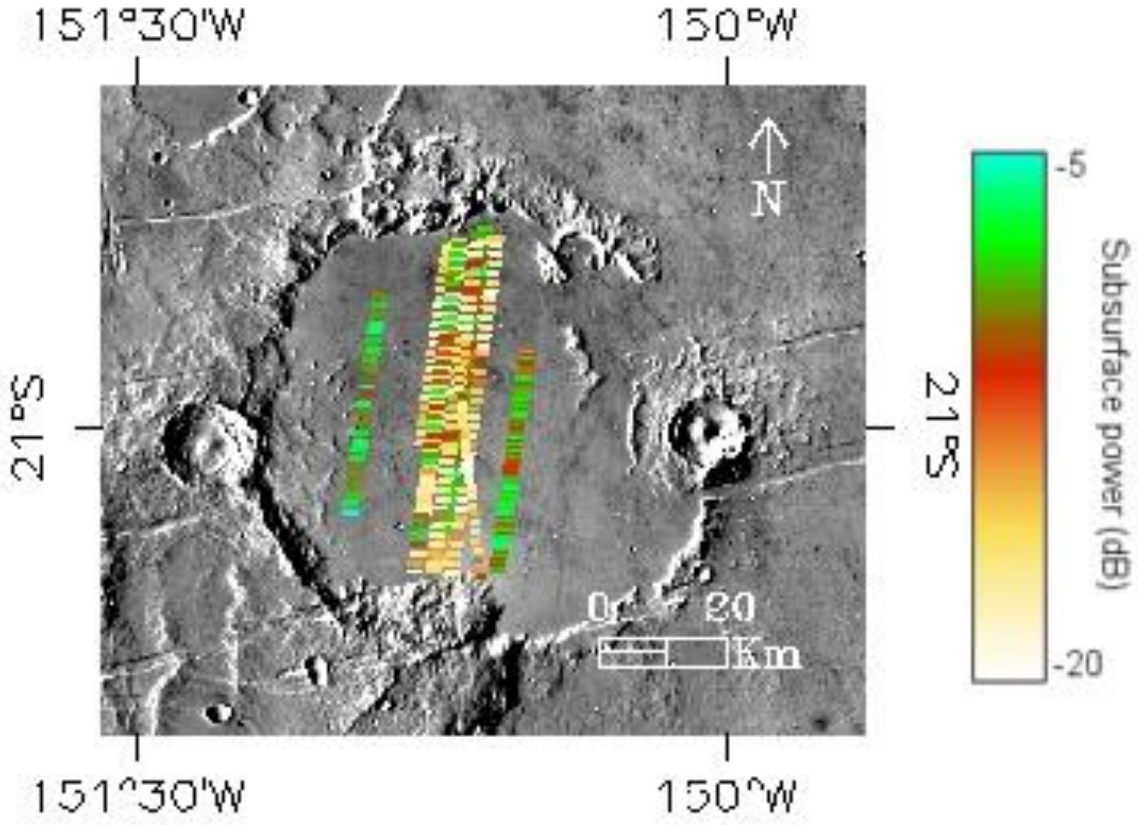

Figure 4.5 Daytime THEMIS image draped over MOLA hillshade image. SHARAD ground tracks illustrate subsurface power in dB of the prominent subsurface detections over the Lal crater.

Most of the subsurface reflections extend the entire diameter of the crater and are centrally located along the north-south axis. They are not detected near the eastern and western rims of the crater. The time delay between the surface to subsurface reflections changes minimally, indicating that the subsurface interface has a low slope and is mostly conformable with the low-slope surface topography (Figure 4.6).

The majority of radargrams at Lal crater detect a single subsurface reflection. However, at some locations, second subsurface reflectors are detected, indicating the presence of at least four distinct vertical geologic units (Figure 4.6).

The second reflector is near-parallel to the first reflector. Because the original crater floor should be bowl-shaped, so a possible interpretation of this geometry is to reveal that subsurface infilling occurred in this region in at least four events, with the possibility of many prior infilling events that remain undetected by SHARAD. The one-way time delay between the first and second subsurface reflectors is small (~0.3 μs on average), indicating a unit of 30 to 40 m thick for the assumed $\varepsilon = 8$ and $\varepsilon = 5$, respectively. These two units represent the final infilling events of the Lal crater, but no interpretation can be made about the time span between these subsequent infilling events.

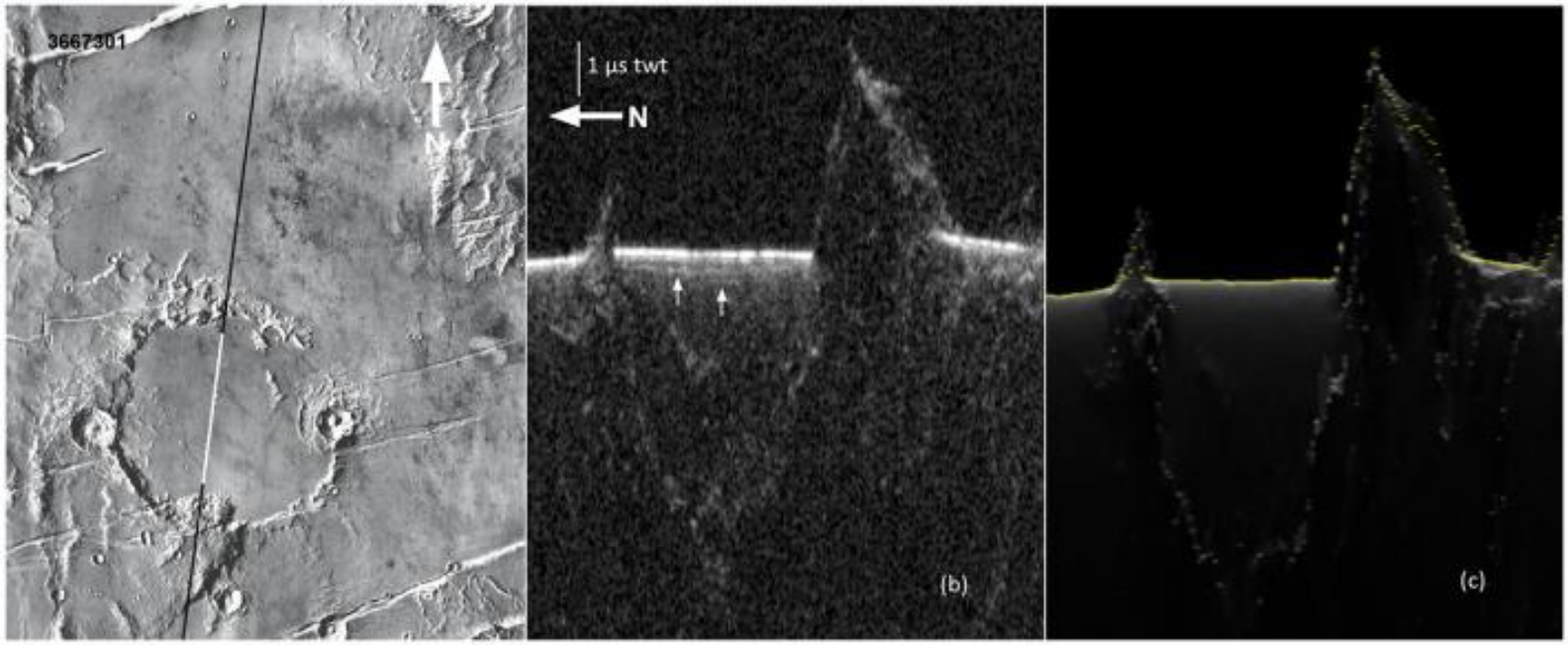

Figure 4.6 Detection of multiple subsurface reflections from within the Lal crater: Daytime THEMIS image (a) corresponding to the SHARAD ground track (Orbit No. 3667301, black line); the white patch over the track refers to subsurface reflection. These have no corresponding reflection in the simulated radargrams (c), demonstrating their subsurface nature (b).

4.3.2 Loss tangent

Here, the best fit of the loss tangent has been derived using the methods described in Section 2.2 (Eq. (1)); however, the range of time delays obtained within a single radargram is small and does not yield a good fit of slope vs. time delay. To mitigate this issue, at another location, Carter et al. (2009) combined data from nearby tracks to get a more reliable fit. Following this method, here, the reflectors from two radar tracks were combined to increase the total range of time delays and derive a reasonably better fit (Figure 4.7). There is little variation observed in the surface echo power of the different orbits, therefore normalization of the surface power is not required. There is some potential error involved with changing roughness within each track (Carter et al., 2009), but our study region appears very smooth in the images.

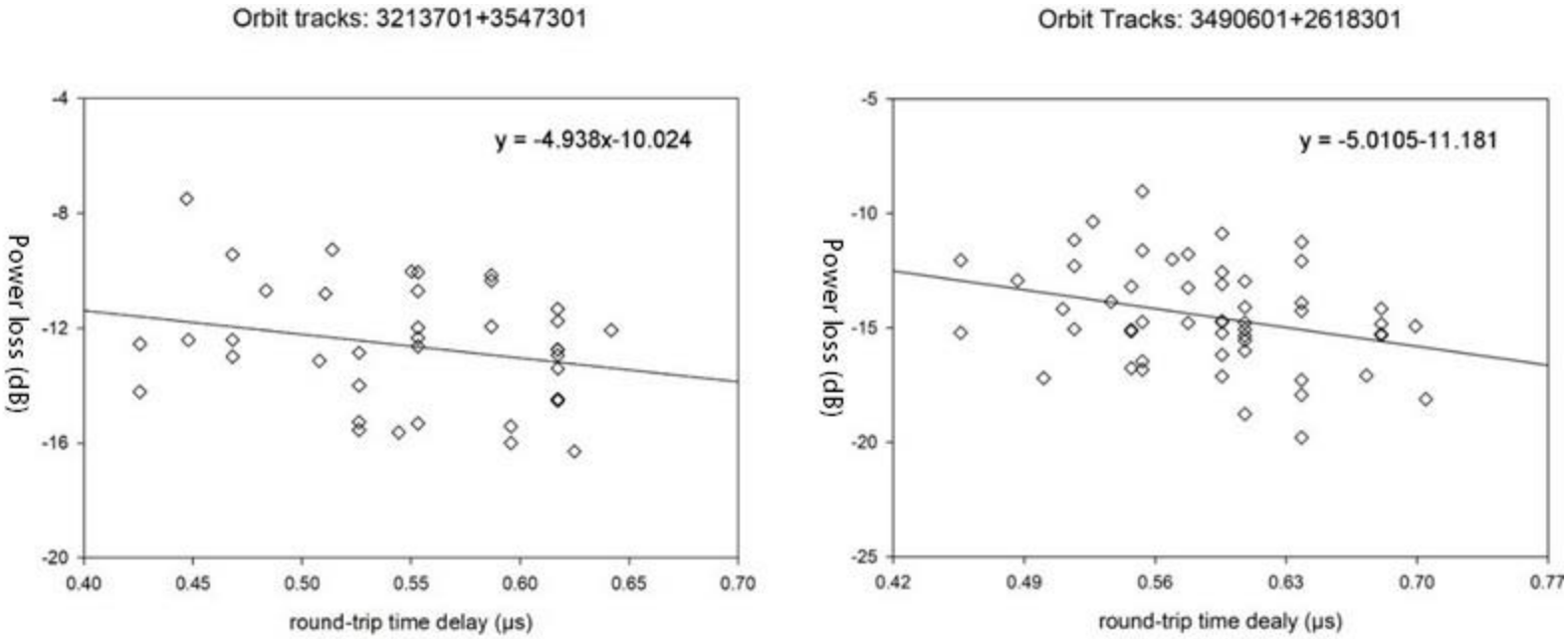

Figure 4.7 A scatter plot showing the SHARAD subsurface reflector power loss (in dB) as a function of round-trip time delay for the tracks over the Lal crater. The solid line represents the best linear fit of power loss and time delay.

Using Eq. (1), the obtained loss tangent values range between 0.008 and 0.009 (Table 4.1). These values are consistent with a low to moderate radar absorbing material like dry, moderate density sediments or basalts exhibiting lower end of the measured range (Campbell et al., 2008).

Table 4.1: Signals power loss (dB/μs), and derived Loss Tangents

Obs. Nos.	Intercept (dB)	Slope (dB/μs)	SD of Slope	Loss Tangent
3490601+2618301	-11.1	-5.01	0.05	0.009
3213701+3547301	-10.02	-4.93	0.07	0.008 – 0.009

4.3.3 Dielectric constant

The dielectric values for the subsurface reflector, i.e., ε_{ss} (4.8) material, is derived from Eq. (7). Using the relative power of the surface and subsurface reflectors, the ratio between the power reflectance (P_{ss}/P_s) can be calculated and the round-trip time delay in radar observations to the subsurface reflection can be included. The observed parameters have been listed in Table 4.2 for the eight distinct orbit tracks across the Lal crater. In reflections from the crater, a two-way time delay for Interface 2 is observed to vary from 0.4 μs to 0.7 μs, implying a nearly flat subsurface reflector. The reflectors amplitude varies from −9 dB to −18 dB, and the range of P_{ss}/P_s is between 0.13 and 0.01.

Table 4.2: SHARAD observations for the crater subsurface reflections

SHARAD Obs. Number	Power Loss in dB	Two Way Time (twt) in μs	P_{SS}/P_S
3667301	−11.1 to −18.5	0.40–0.68	0.078–0.014
2570201	−10.7 to −17.4	0.41–0.65	0.085–0.018
2618301	−12.04 to −17.04	0.45–0.57	0.063–0.020
2648001	−9.4 to −17.2	0.42–0.63	0.115–0.019
3213701	−9.2 to −16.2	0.44–0.64	0.120–0.024
3455001	−9.0 to −15.3	0.39–0.63	0.125–0.029
3490601	−9.0 to −18.1	0.51–0.70	0.126–0.015
3547301	−9.4 to −18.5	0.42–0.59	0.115–0.014

A range of possible values of ε_{ss} vs. P_{ss}/P_s are plotted in Figure 4.8(a) for the subsurface reflection based on Eq. (7) and assuming dielectric values $\varepsilon_s = \varepsilon_l = 7$ and 8 for lava (a range obtained by Carter et al., 2009; Simon et al., 2014). The derived subsurface dielectric constant (ε_{ss}) fits well in the range of ~4.6–6.1 (average = 5.35) for $\varepsilon_s = 7$ (red filled circles) and 5.1–6.9 (average = 6.0) after using the $\varepsilon_s = 8$ (black filled circles). However, my calculation also suggests that the value of the subsurface dielectric constant decreases further if $\varepsilon_l < \varepsilon_s$ (Figure 4.8b). In this calculation, ε_s remain constant, but the value of εl is varied.

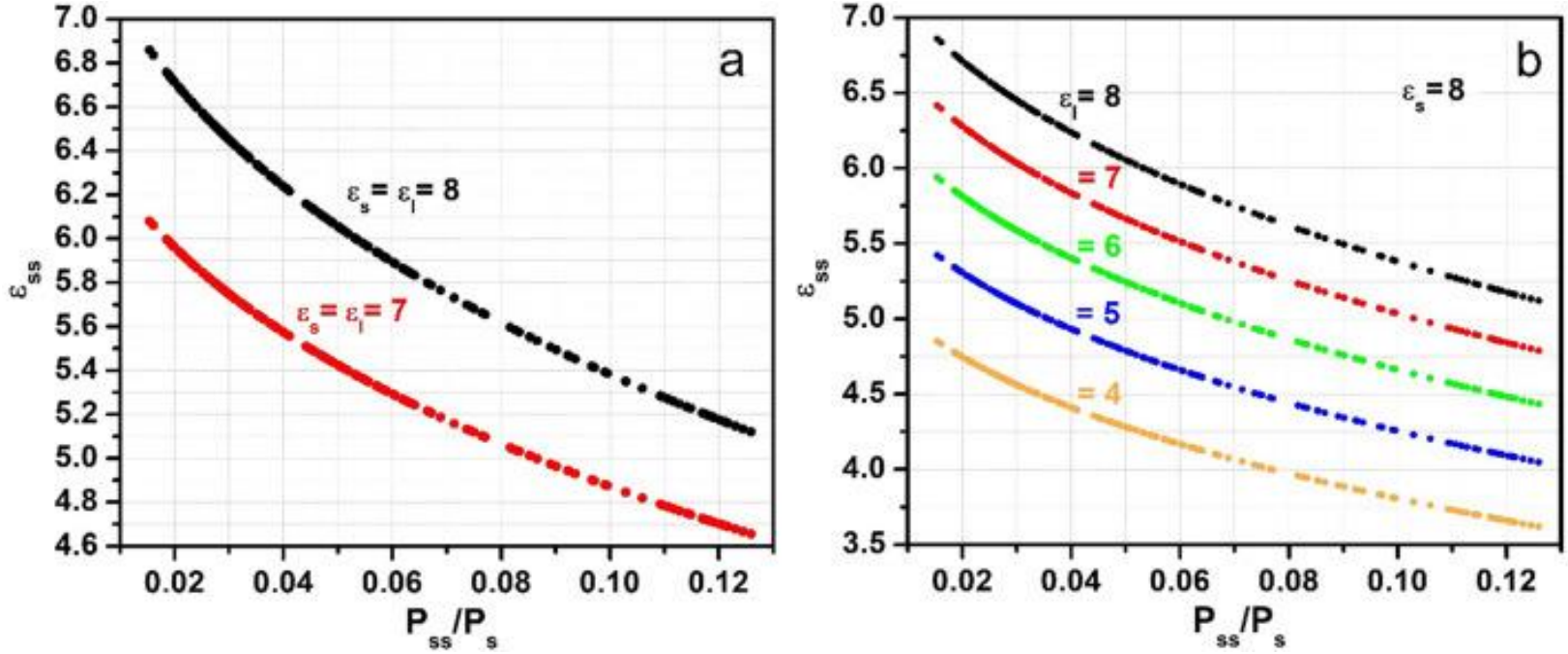

Figure 4.8 Subsurface dielectric permittivity (ε_{ss}) estimates vs. P_{ss}/P_s for the subsurface reflections from within the Lal crater. ν = 20 MHz, and ε_o = 1 have been used. Panel (a) corresponds to $\varepsilon_l = \varepsilon_s$, whereas panel (b) refers to $\varepsilon_l \leq \varepsilon_s$.

Previous studies have reported dielectric constants of the geologic material from 3 for ice and 3–6.5 for porous sedimentary material to 8 for dense basalt (Campbell and Ulrichs, 1969; Ulaby et al., 1988; Carrier et al., 1991). In this study, the derived dielectric constant lies within a range that is most consistent with moderate density sediment (ε = 3 to 6.5, Ulaby et al., 1988) rather than the dense basalt. Considering the two-way time delay corresponding to the crater reflections and using the calculated mean dielectric permittivity values 5.35 and 6 along with Eq. (2), it is estimated that the thickness *d* of the subsurface layer of unknown composition is ~44–47 m.

4.4 Discussion

4.4.1. Hypotheses about the origin of the reflector

The surface exposure in the central and eastern portions of the crater is considered as an early Hesperian volcanic unit of an unknown thickness (Tanaka et al., 2014). This interpretation is used to inform our model and assume that the uppermost unit in this area is a lava unit. Radar theory does not permit a reflection between two subsurface materials of the same dielectric properties; therefore, the dielectric contrast between the first and second subsurface reflections (bounding the subsurface unit ε_{ss}, immediately below the top lava surface ε_s) must be explained. Three hypotheses are given for the origin of these reflectors based on earlier studies of the Mangala region (Crumpler and Aubele, 1978; Zimbelman et al., 1992; Cattermole, 2001; Head and Wilson, 2001; Ghatan et al., 2004; Head et al., 2004; Wilson and Head, 2004; Leask, 2005) and the SHARAD investigations of the Lal crater.

Hypothesis 1

Morgan et al. (2015) studied subsurface reflectors in Elysium Planitia between stacked lava flows (of similar dielectric values) and interpreted the reflections to indicate that dust or another low-density material, likely the highly friable Medusae Fossae Formation material, was sandwiched between lava flows. Similar to the Elysium Planitia, the entire Tharsis region is covered in dust (Christensen, 1986), and surface wind streaks are common in the Mangala region (Thomas et al., 1981; Lee et al., 1982), showing transport of low-density material at today's surface. Therefore, my first hypothesis is that dust could be sandwiched between layers ε_s and ε_{ss} at Interface 1 in the Lal crater. Because of its analogous behavior with Elysium Planitia and paucity of reflections between lava flows elsewhere on Mars, this may be a plausible scenario for causing the reflections. This would be consistent with an interpretation of stacked lava layers with a thin interbedded layer of ash and inconsistent with lava over sediment.

Hypothesis 2

The reflection may arise from contrasts between successive lava flows interbedded with ejecta material from the Hilsa and Mursan superimposed craters situated on the eastern and western rims of the Lal crater. The craters situated in this area and those superimposed on the Lal crater rim have lobate ejecta blankets, possibly indicating the presence of subsurface volatile at the time of crater formation (Carr and Schaber, 1977; Tanaka and Chapman, 1990; Squyres et al., 1992; Zimbelman et al., 1992; Ghatan et al., 2004). The embayment of the ejecta blankets within the Lal crater by the final infilling unit implies that at least the uppermost unit lies above the

extensive ejecta. It may be possible that ejecta material, most likely dry and low-density rubble, is embedded between successive lava flows, creating a dielectric contrast.

Hypothesis 3

Sedimentary material from the nearby highland units (eNh and mNh) and Lal crater rim erosion may have been deposited inside the crater during the period of high erosion, leaving a lower density unit between successive lava flows in the east and central portion of the crater. This hypothesis would be consistent with the interpretation that sedimentary material partially filled the crater (Tanaka et al., 2014), remaining exposed in the west but covered by later lava flows from the east.

4.4.2 Hypothesis testing

Essential aspects to consider while hypothesis testing is the relatively low values of tanδ and ε' associated with the subsurface unit. Carter et al. (2009) measured the loss tangent and dielectric value near the northwest of the Ascraeus Mons. They found that the range of the loss tangent is 0.01 to 0.03, and the average measured dielectric constant is 12.2 and 9.8. Simon et al. (2014) studied the lava flows northwest of Ascraeus Mons, west of Ascraeus Mons, and south of Pavonis Mons and obtained loss tangent ranges of 0.007–0.029 and dielectric constant with an average value of 9.6. Comparing the results with these studies, it is inferred that the material of the radar observed subsurface unit at Lal crater is inconsistent with lava. Thus, the first hypothesis, wherein the reflector was composed of lava, can be excluded.

The second hypothesis suggests that the superimposed crater's lobate ejecta material embedded between successive lava flows may be creating the dielectric difference. These superimposed craters are ~12 km in diameter, and their ejecta blankets from the rim may extend up to ~25 km towards the center of the Lal crater. In terms of crater radius (R_C), half of the ejecta material could be deposited within $1R_C$, and most of the ejecta material (>90%) within 5 R_C from the rim of an impact crater (Melosh, 1989, p. 90; French, 1998). This implies that >90% of the superimposed craters' ejecta material may be deposited within 25 km from the rim of the craters. The ejecta thickness near the crater rim towards the center of the Lal crater, using the semi-empirical formula to measure the thickness of lunar crater ejecta (McGetchin et al., 1973), varies in the range of 90 m at the crater rims to 2 m near the center of the Mangala crater. Figure 4.5 demonstrates that the subsurface reflections are observed only in a narrow region towards the center of the Lal crater. If it is assumed that the ejecta blanket is present at the center of the crater, then its thickness can be only ~2 m, significantly lower than our measured thickness (~44–47 m). Thus, the evidences do not support the second hypothesis of crater ejecta forming the interfaces.

The third hypothesis is the infilling of sedimentary material that probably took place during erosion of the crater rim and the highland units located in the region surrounding Lal crater (Figure 4.1). These highland units, namely, eNh and mNh, are described with the composition of undifferentiated impact, volcanic, fluvial, and basin materials (Tanaka et al., 2014). Morphological evidence, including the final burial of the fossae

surface exposures, suggests that the smaller fossae connecting to the highland unit and Lal crater were active even after the formation of the Hilsa and Mursan superimposed rim craters. They might have served as the transportation channel that fed the sedimentary deposit. There is evidence of late fluvial activities (Zimbelman et al., 1992; Head and Wilson, 2001; Ghatan et al., 2004; Head et al., 2004; Wilson and Head, 2004; Leask, 2005; De Hon, 1992, De Hon, 2010), significant amounts of water-equivalent hydrogen-rich soils (Feldman et al., 2004), and evidence of Martian valley network (Hynek et al., 2010; Kite et al., 2019) present in the Mangala region. Also, evidence of lobate, "muddy" ejected material is present around the crater on both the north and south side of Mangala Fossa (Leask et al., 2007). The nature of the ejecta strongly suggests that a cryosphere existed in this area at the time of crater formation (Carr and Schaber, 1977; Tanaka and Chapman, 1990; Squyres et al., 1992). Based on these investigations and SHARAD-based results, it is concluded that the third hypothesis is most consistent with the derived dielectric constant.

4.4.3 Compositional constraints

After testing the hypothesis, it becomes important to constraint the composition of the infilling material. Power loss in terms of dB/μs can be observed with radar wave propagation from the surface to the subsurface. A rate of decrease of ~5 dB/μs with two-way echo has been observed in this study while the observed power loss in ice is ~2 dB/μs for the real dielectric constant of 3 (Plaut et al., 2009) and ~ 13 dB/μs in basalt for dielectric constant in the range of 6.2–17.3 (Carter et al., 2009). Thus, power loss is moderate in the Lal crater, and it is comparable with the ~5 dB/μs power

loss in Vastitas Borealis Formation (VBF) material in Amazonis Planitia (Campbell et al., 2008). This comparison of power loss indicates that the infilling of material infilled in the Lal crater is a low radar absorbing material with an average dielectric value of ~5.35–6.0. Electrical properties of the subsurface reflector of the Lal crater suggest that the subsurface deposit is more consistent with the VBF material of Amazonis Planitia.

4.4.4 Volume of the infilling material

The initial crater depth, i.e., the post-modification crater depth in km from the rim, can be defined as $d_r = 0.357\ D^{0.52}$, where D is the crater diameter (Tornabene et al., 2013; Bamberg et al., 2014). Using this equation, the d_r estimation of the Lal crater from rim to craters bottom is ~3.13 km, where D ≈ 65 km. Subtracting the current average height of the rim (h_r ≈ 370 m, MOLA stats) over the central deposit gives a total depth of $d = d_r - h_r \approx 2.76$ km. Hence, the lowermost units of the Lal crater (below the lowest detected radar reflector) may have contributed up to 2.76 km to the infill. The crater volume may be expressed as $V_c = (\pi d/12)\ (3D^2 - 4d^2)$. This refers to the total crater infilling volume up to 9136 km^3 for $D \approx 65$ km and $d \approx 2.76$ km. The subsurface layer volume with diameter s and thickness p may be approximated as $V_{s1} = (\pi/4)\ s^2 p$. The ratio of the two may be expressed as, $(V_{s1}/V_c) = (3/d)\ s^2 p\ (3D^2 - 4d^2)^{-1}$, where s = 65 km and p = 45 m, giving $V_{s1} / V_c = 0.0062$. Thus, the sedimentary layer occupies ~1.64% of the total crater volume or ~ 150 km^3.

Furthermore, in this context, it would be interesting to comment on Figure 4.6, where two subsurface reflections are observed within the Lal crater. The time delay between the first and the second subsurface reflectors

is small (~0.3 μs on average along with the detection), indicative of a thin unit. However, without further information about the appropriate dielectric properties of the material between the subsurface reflectors, no calculation has been made for the volume for the second reflectors.

4.5 Conclusions

Using SHARAD observations, multiple subsurface reflections within the Lal crater have been observed. Based on our analysis, the first subsurface reflector is caused by contrasts from moderate density sedimentary material with the loss tangent in the range of 0.008–0.009 and has a mean dielectric value of ~5.35. These values are lower than the values calculated for lava layers in the Tharsis region (loss tangent 0.01 to 0.03 and $\varepsilon \sim 6.2$–17.3, Carter et al., 2009), and more in line with Vastitas Borealis Formation (VBF) material of Amazonis Planitia, which has loss tangent in the range of 0.005–0.012 (Campbell et al., 2008), and it is interpreted as sediment. The derived loss tangent and dielectric values are consistent with the sedimentary origin hypothesis and cited morphological evidence of past geological activities in this region. The source of the sedimentary deposit may be the surrounding highland units and the rim of the crater in the late Hesperian period. The volume calculation shows that the subsurface unit (ε_{ss}) occupies approximately 150 km^3 or ~1.64% of the Lal crater by volume, and its thickness is ~44–47 m. The observation of two subsurface reflections within the crater indicates that infilling occurred in at least four events; however, it is difficult to draw conclusions about the total number of infilling events prior to deposition of the lowermost reflector. In summary, this study shows that in contrast to the primary emplacement of lava in the Tharsis

region, the Mangala Fossa region has experienced episodes of both, lava flow and erosion that deposited sediments in a large basin and it demonstrates that a significant quantity of the sedimentary material is buried by lava units in the Lal crater.

Chapter 5

Subsurface study of the Tharsis graben system

5.1 Introduction

Numerous grabens extend radially away from the Tharsis Montes (Wise et al., 1979a, 1979b; Plescia and Saunders, 1982; Wilson and Head, 2002), and they extend in the range of a few hundred meters to thousands of kilometers (Figure 5.1A). Geological maps and crater counting confirm their existence throughout the Noachian to Amazonian periods (Scott and Tanaka, 1986; Tanaka et al., 1992, Tanaka et al., 2014), yet the formation process is still elusive. Two hypotheses emerged from the earlier studies for the formation process of these graben systems: i) tectonic process (crustal extension) only (Plescia and Saunders, 1982; Banerdt, W.B. et al., 1992; Phillips, R.J. et al., 2001), and ii) magmatic and tectonic processes where extension and dikes both are involved (Mège, D., and Masson, P., 1996; Ernst, R.E. et al., 2001; Wilson, L., and Head, J.W., 2002; Scott et al., 2002; Mège, D. et al.2003). The first hypothesis emerged from large-scale volcanism and extensive fracturing resulting from the loading of the lithosphere by voluminous extrusive and intrusive magmatic deposits in the Tharsis region (Zuber, 2001; Phillips, R.J. et al., 2001). The second hypothesis involves the underlying dike injections and dike swarms in the grabens formation process (Mège and Masson, 1996b; Ernst et al., 2001; Wilson and Head, 2002; Scott et al., 2002; Head et al., 2003; Mège et al., 2003; Schultz et al., 2004). A model study suggests that the forcible widening by dikes alone is not sufficient to produce a graben at the surface (Wyrick and Smart, 2009). But, another study by Schultz et al., 2004 conclude that the Memnonia graben system (located south of and parallel to Mangala Fossa) is most consistent with a dike-induced origin and least compatible with a

faulting-based origin, but they also observed that the other Tharsis radial grabens do not consistently reveal dike-related topographic signatures. Most of these studies used topography data or modeled the formation process using crustal mechanics and fluid dynamics, but subsurface radar data was used for the first time in this study to obtain new evidence that can be used to validate these studies.

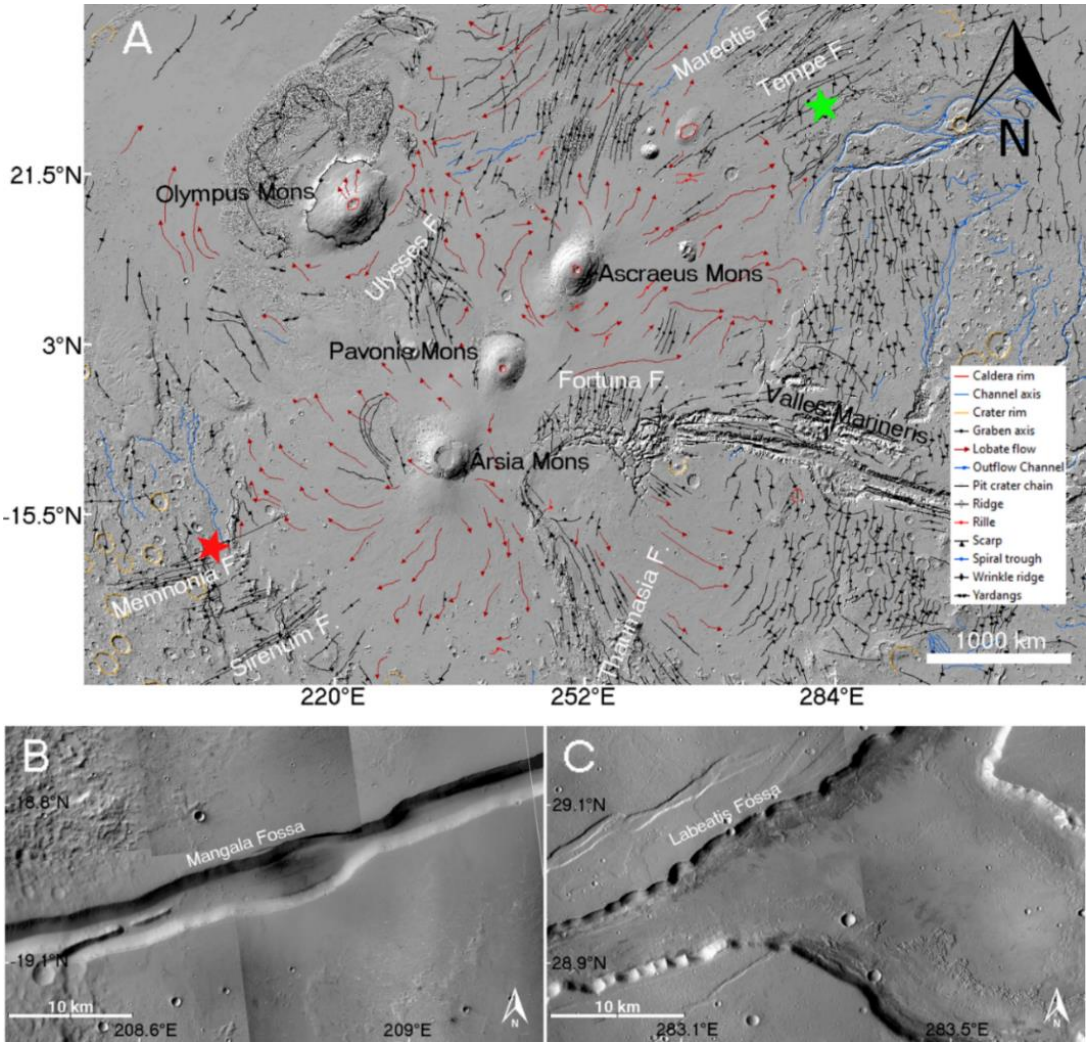

Figure 5.1 (A) Geologic map of the Tharsis region using MOLA topography data. Layers of geological features in this map are taken from Tanaka et al. 2014. Black lines with circular dots in the middle are graben axis. Red and green star represents the location of the study areas (B) Mangala Fossa and (C) Labeatis Fossa, respectively. In Figures 5.1 B and C Context (CTX) high-resolution images have been used.

The geological context and subsurface of Mangala Fossa (Figure 5.1B) and Labeatis Fossa (Figure 5.1C), have been studied using data from CTX and SHARAD onboard MRO, and THEMIS aboard Mars Odyssey. SHARAD can detect dielectric discontinuity, if any, up to several meters into the subsurface. The dielectric discontinuity is observed as a reflection in terms of power (dB) vs. time delay (μs) in radargram. This observation is used to determine the reflection geometry, attenuation rate, and loss tangent, which help us to decide the material's properties. The extent of infilling is also mapped on the basis of the observed subsurface reflections. Finally, possible mechanisms for the emplacement of material have been identified, which help us to understand the formation process of these graben systems.

The Mangala Fossa and the Labeatis Fossa are diagonally opposite to the Tharsis Montes (Figure 5.1A). The Mangala Fossa, a 695 km long SW trending graben (U.S. Geological Survey, 2003), is located in the Northernmost part of the Memnonia Fossae (Figure 5.1A). It is the source of Mangala Valles, a major outflow channel interpreted as a result of dike-induced formation (Head et al., 2004). Dike outcrops are visible on the floor of Mangala Fossa and Mangala Valles (Leask et al., 2007; Basilevsky et al., 2009). Labeatis Fossaa, a series of NE trending grabens of Tempe Fossae, is situated towards the northeast of the Tharsis Montes and in the SW region of Tempe Terra and Tempe Fossae (Figure 5.1A). Unlike in the Mangala region, there are no visible dike outcrops in this region. Extensive radial normal faulting occurred in this area and extended outward at Tempe Terra (Tanaka et al., 1992).

Most of the Martian grabens systems are narrow structures, so radar interpretation is complicated by the presence of clutter (explained in Sec.2.1). The two sites in this study benefit from their setting. The surrounding of Mangla Fossa is a smooth plane where clutter is minimal. The channel of Labetais Fossa is broad and smooth enough that SHAHRD can probe the subsurface without generating too much clutter (Figure 5.1C). There is also ample coverage of these area by SHARAD for interpretation. Subsurface reflections have been found at the rim of the Mangala Fossa and at the floor of Labeatis Fossa (Figure 5.3), which can help to investigate and unravel the formation process of these two graben systems and potentially offer value for interpreting fossae elsewhere on Mars.

5.2 SHARAD Observations & Derivatives

5.2.1 Analysis

Analysis of orbital radar data requires distinguishing between clutter, or signals from the surface. Signals away from the nadir point that arrive at the same time delay as desired subsurface signals, generate clutter. To identify the clutter, the Colorado SHARAD Processing System (CO-SHARPS, Putzig et al., 2016) has been used to generate cluttergrams (Choudhary et al., 2016) for comparison with the SHARAD radargram (Figure 5.2).

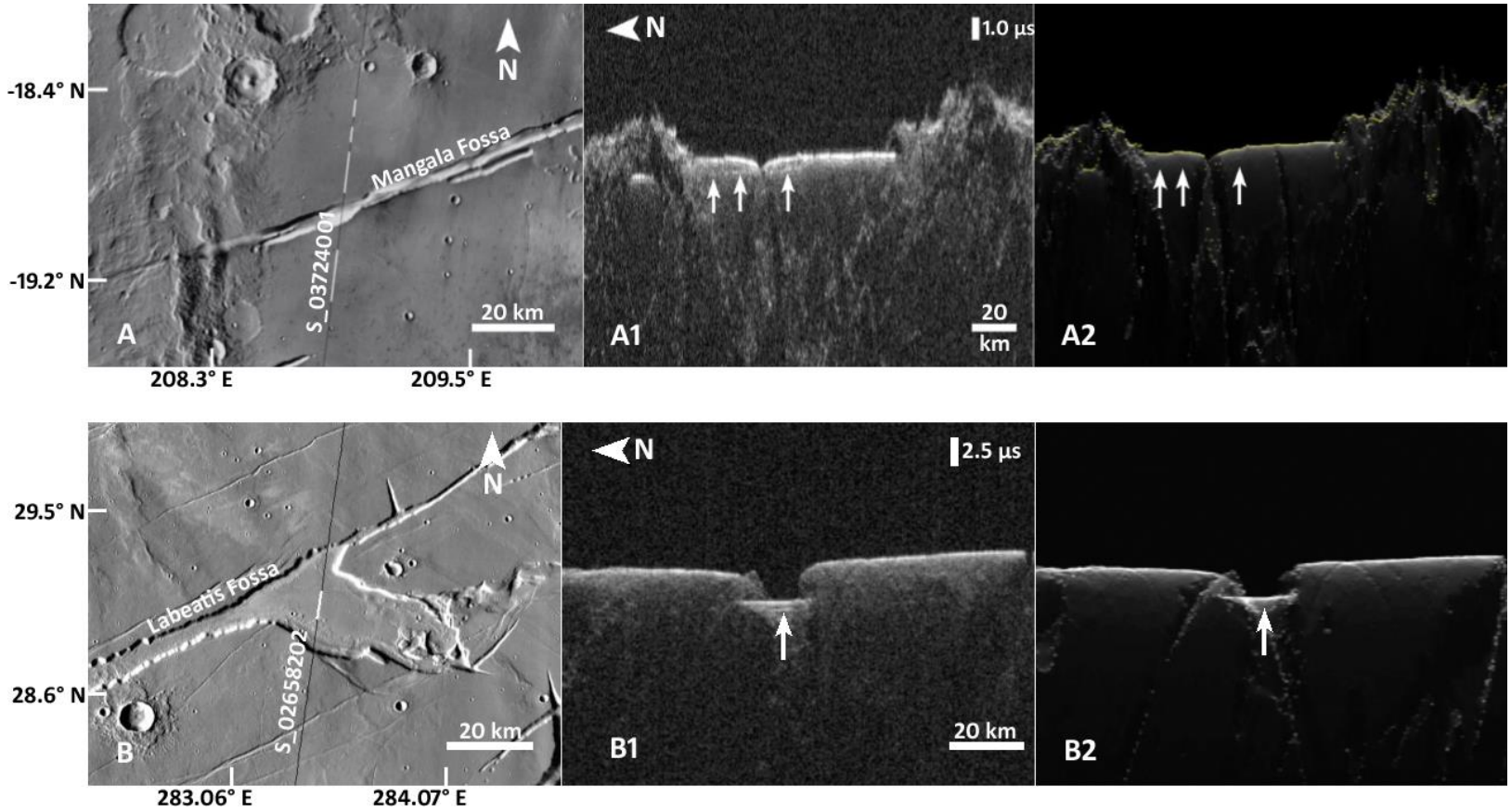

Figure 5.2 SHARAD ground track in black overlying the Thermal Emission Imaging System (THEMIS) daytime IR mosaic (A: Mangala Fossa and B: Labeatis Fossa). The white band on SHARAD ground track in A and B indicates the location of each subsurface reflection. SHARAD radargrams (A1 and B1) have white arrows indicating subsurface reflections associated with the graben. Clutter simulations (A2, B2) that correspond to the SHARAD observations find no predicated clutter at the same time delay (no reflections at white arrows).

White bands on the SHARAD footprints (black line) in Figure 5.2A and 5.2B identify the locations of subsurface reflections at the rim of Mangala Fossa and at Labeatis Fossa floor, respectively. White arrows (Figure 5.2: A1 and B1) indicate the subsurface reflections, which are not apparent in the corresponding cluttergarm (Figure 5.2: A2 and B2). Figure 5.3 shows the distribution map of the clutter-mitigated subsurface reflections at the rim of the Mangala Fossa (Figure 5.3A) and within Labeatis Fossa (Figure 5.3B).

The subsurface reflections at the rim of Mangala Fossa have a narrow range of time delays which is in the range of 0.3 μs to 1.6 μs (Figure 5.3A). Reflections at the floor of Labeatis Fossa have a relatively flat geometry as evidenced by the round-trip time delay in the range of 0.7 μs- 1.2 μs (Figure 5.3B).

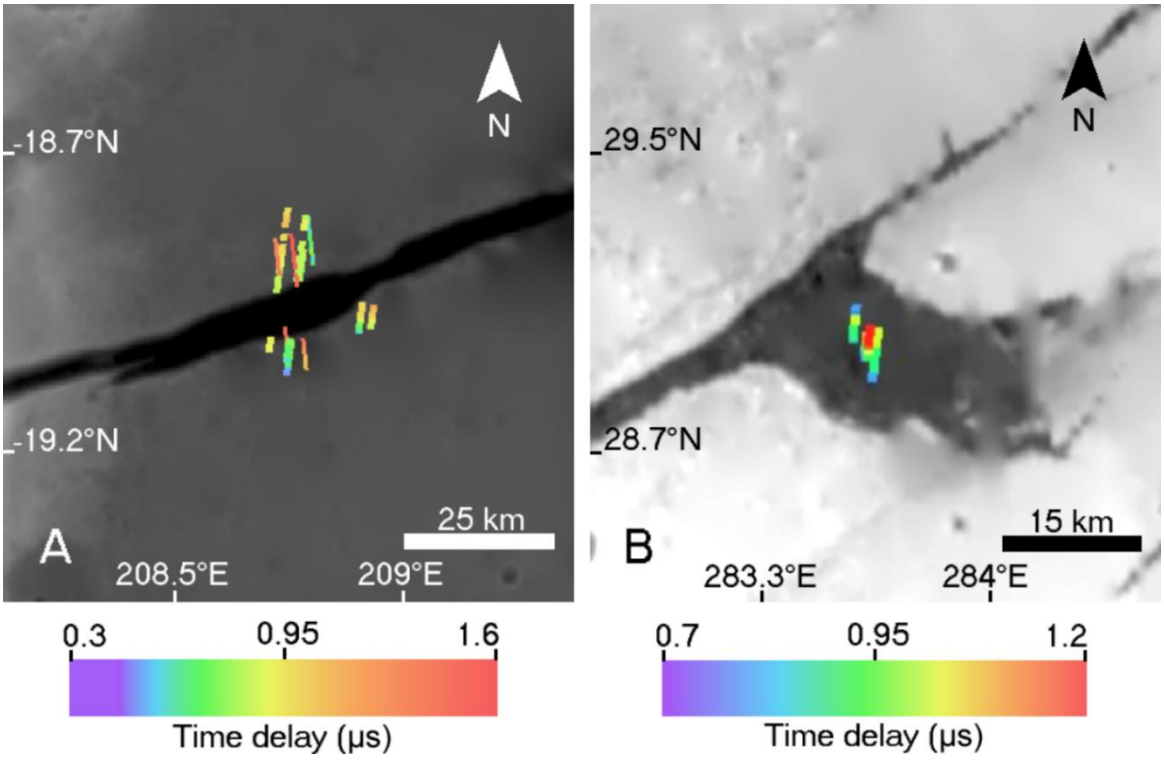

Figure 5.3 SHARAD subsurface reflection distribution map of the study regions laid over HRSC and MOLA Blended Digital Elevation Model at 200m data. A: Mangala Fossa and B: Labeatis Fossa. SHARAD ground track colors illustrate the two-way time delay of the reflections over the region.

5.2.2 Radar wave attenuation

The attenuation rate of amplitude from the surface to the subsurface (measured in dB/μs) is an essential geophysical property of the subsurface material in radar propagation theory (Plaut et al., 2009; Campbell et al., 2008; Carter et al., 2009; Bharti et al., 2022). The along-track power of reflector (surface and subsurface) of SHARAD observations that cross Mangala Fossa and Labeatis Fossa has been measured to characterize the signal sensitivity in terms of the power loss (dB) and time delay (μs). Then scatter plots (Figure 5.4) were used to obtain the best empirical linear fit to determine the power

loss (dB/μs) between the surface to subsurface reflection by measuring the slope of the plot.

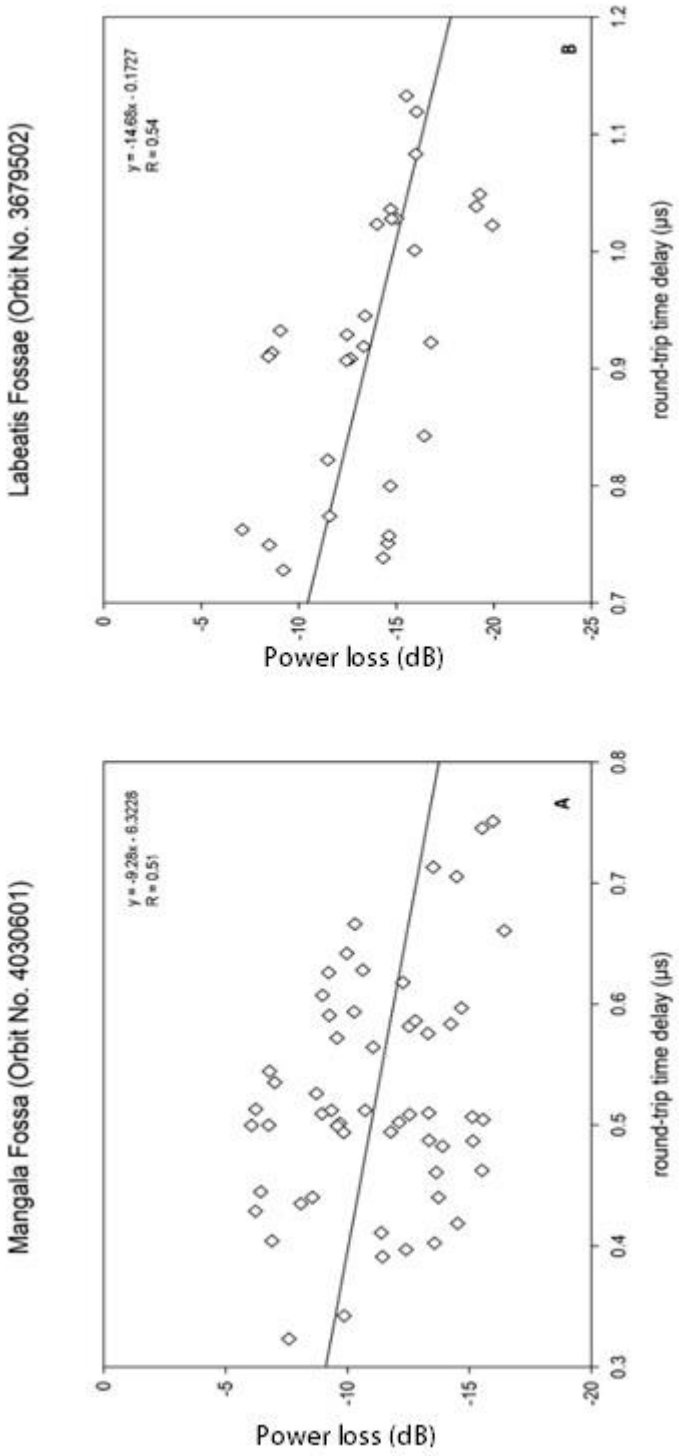

Figure 5.4 SHARAD power loss (in dB) versus round trip time delay (in μs) for (a) orbit no. 4030601 at Mangala Fossa rim, and (b) orbit no. 3679502 at the floor of Labeatis Fossa.

An attenuation rate of -9.28 dB/μs is calculated using the best empirical linear fit in the Mangala Fossa (Figure 4A), while -14.68 dB/μs is obtained for Labeatis Fossa (Figure 4B) region. This is in line with previous SHARAD studies of the lava flow in the Tharsis region, including the west of Ascraeus Mons, which have obtained an attenuation rate in the range of -2.43 to -15.7 dB/μs (Carter et al., 2009; Simon et al., 2014). The derived attenuation rate of the study regions is comparable with the middle to upper range of the Tharsis region lava flows, which suggests a low to moderate concentration of radar-wave absorbing lava unit comprises the uppermost geologic layer.

5.2.3 Loss tangent

The loss tangent corresponding to the subsurface transmission loss can be expressed as,

$$tan\delta = \left[\left(2\left(\frac{\lambda}{4\pi c \Delta \tau}(lnL) \right)^2 + 1 \right)^2 - 1 \right]^{1/2} \quad (1)$$

where L is the power loss per unit time Δτ at the λ=15 m SHARAD wavelength, and c refers to the speed of light of 300 m/μs in a vacuum (Campbell et al., 2008). This formulation assumes that the surface and subsurface roughness are roughly equal and constant and that their respective dielectric constant is same over the measurement area (Carter et al., 2009). After considering the standard deviation of the best fit, the loss tangent values were calculated to be in the range of 0.009 to 0.02 at Mangala Fossa and 0.01 to 0.03 at Labeatis Fossa (Table 5.1). These values

are consistent with two SHARAD studies of Tharsis lava units, which calculated loss tangent values in the range of 0.007 to 0.03 (Carter et al., 2009; Simon et al., 2014).

Table 5.1 Loss Tangent value at Mangala Fossa and Labeatis Fossa

Track Number	Location	Intercept (dB)	Slope (dB/μs)	SD of Slope	Loss Tangent*
4030601	Mangala Fossa	-6.32	-9.28	3.9	0.009-0.02
3679502	Labeatis Fossa	-0.17	-14.68	3.7	0.01-0.03

*Loss tangents range is computed from 1σ fitting error in the slope.

In the absence of an independent means to constrain the depth of reflectors identified in the SHARAD data, derived dielectric constants have been used to estimate the thickness of these subsurface units. Because the calculated power loss and loss tangent values in my study are comparable with values from previous studies of the Tharsis lava units (Carter et al., 2009; Simon et al., 2014), it is assumed that the units in this study have matching dielectric constant range of 9.6-12.2. Thus, the thickness can be computed using relation:

$$h = \left(\frac{c\Delta t}{2\sqrt{\varepsilon'}}\right) \quad (2)$$

where c is the speed of light in vacuum, Δt is the two-way time delay between the surface and subsurface echoes measured from the radargram,

and ε' is the real part of the dielectric value of the subsurface material (Morgan et al., 2015). For the given range of dielectric values (9.6-12.2), the maximum and minimum thickness of the subsurface units are ~39-34m and ~58-51m in the Mangala Fossa and Labeatis Fossa, respectively.

5.3 Discussion

Various studies of surface and subsurface features near the Tharsis region found magma related formations like dikes, pit craters, and subsurface lava flows. Geomorphological studies near the Mangala Fossa and the Labeatis Fossa region reveal dike signatures radiating from Tharsis volcanic shields (Schultz et al., 2004; Leask et al., 2007; Basilevsky et al., 2009). Studies also identified the presence of radial and concentric chains of pit craters in this region. These pit craters have been interpreted as an indication of shallow subsurface dikes (Mège and Masson, 1996, 1997; Liu and Wilson, 1998; Montesi, 1999; Mège et al., 2000; Scott et al., 2000, 2002; Gibbons et al., 2001; Wilson and Head, 2002; Scott and Wilson, 2002). Mege et al., 2003 proposed that there is an interconnection between tectonic and magmatic activities in the Tharsis region. Labeatis Fossa has a pattern similar to the Tractus Catena, where the central trough is surrounded by lateral grabens. This pattern is observed in experimental results when the top of the ductile layer lies above the top of the magma body (Mege et al., 2003).

SHARAD studies of the Tharsis region detected lava flows, mainly near the Tharsis Montes. These flows have common characteristics: flow signatures are visible in the high-resolution topography images, and SHARAD detects a downhill trend with increased time delays from surface to subsurface reflection (Carter et al., 2009; Simon et al., 2014). These

detections help us to understand the flow origin and pattern of the lava flows. Subsurface study revealed that the Tharsis region lava might have frequently been deposited on top of other lava units, and these subsurface lava units are associated with rift zone volcanism (Simon et al., 2014).

The subsurface reflections in Mangala Fossa and Labeatis Fossa are far from the Tharsis Montes. The topography of the reflection is almost flat, as evidenced by a slight variation in the measured time delay between the sub-horizontal surface and the subsurface at these two locations (Figure5.3A & 5.3B). In the next section, an attempt has been made to find out the flow origin of subsurface lava units and to confirm the previous geologic observation as well as the given hypothesis of the formation process of these graben systems using the SHARAD observation.

5.3.1 Scenario of reflection at the rim of Mangala Fossa

High-resolution CTX images show the volcanic surface texture in the surrounding region of Mangala Fossa. Figures 5.5A and 5.5B identify the signature of lava flows near both sides of the fossa rim. These flow characteristics are similar to the observed lava flow features near the Tharsis Montes (Carter et al., 2009; Simon et al., 2014). The observed flows orient outward from the fossa rim and suggests that Mangala Fossa is a possible source of these lava flows. Based on the presence of geomorphic and geophysical evidence, it seems that the SHARAD reflections originate from the basal interfaces of these lava units. The derived loss tangent of these subsurface unit is in the range of 0.009-0.02, consistent with other Tharsis lava unit.

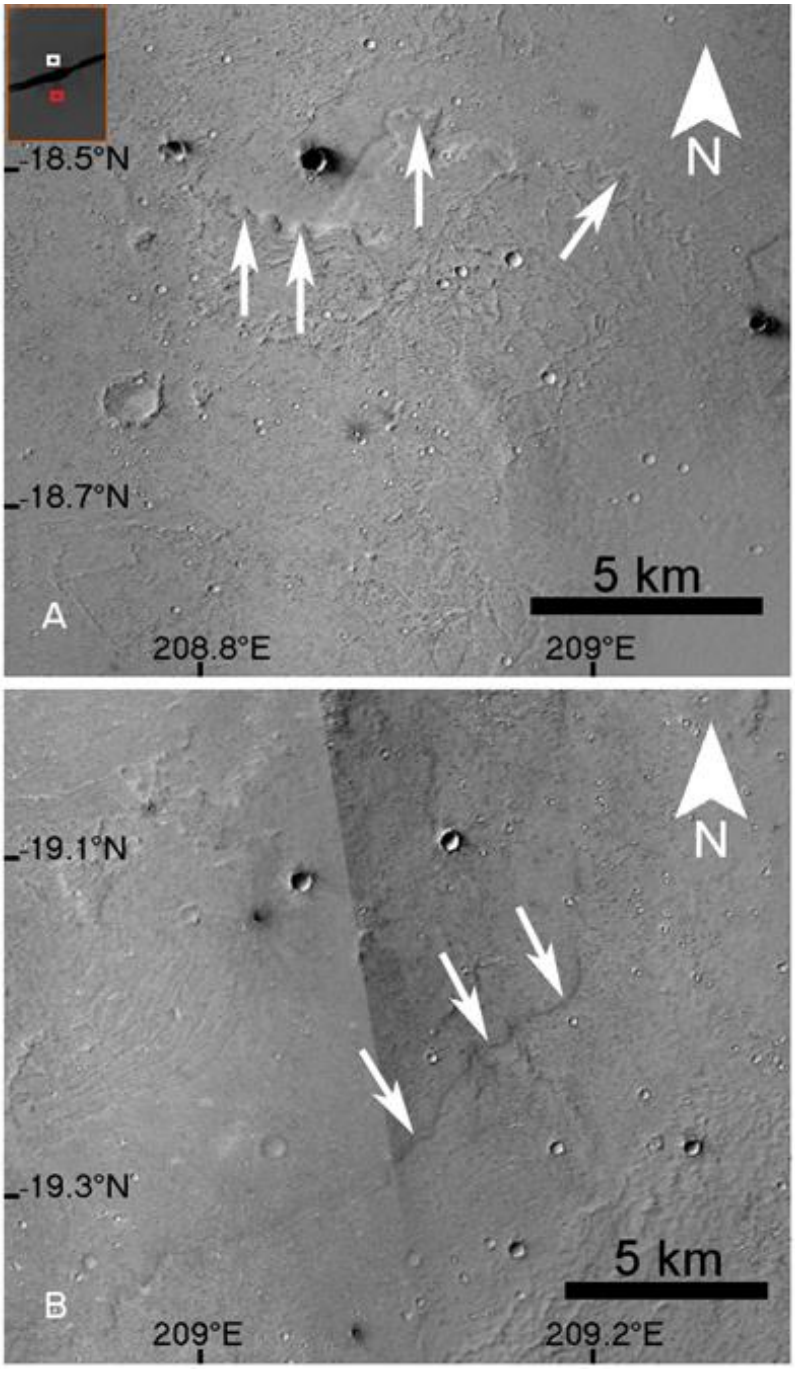

Figure 5.5 CTX images of lava fronts near the Mangala Fossa A: Near the northern rim of Mangala Fossa; B: Near the south rim of Mangala Fossa. White arrows indicate the lobate margin of lava flows and their interpreted flow direction. Inset image of Mangala Fossa: White and red squares represent the location of Figures 5.5 A and 5.5B, respectively.

SHARAD studies near the Tharsis Montes detected similar basal flow interfaces of lava units (Carter et al., 2009; Simon et al., 2014). These interfaces are suggested to be associated with rift zone volcanism (Simon et al., 2014). Some rifts exhibit no volcanic activity, whereas others are highly active and surrounded by vast lava fields (Hancock and Skinner, 2000). The surrounding region of Mangala Fossa is an early Hesperian volcanic (eHv) unit, as mapped in geological map by Tanaka et al. (2014). These units are characterized by flood lava sourced from regional fissures.

The flow pattern of the lava unit (Figures 5.5A and 5.5B) suggests that lava erupted from the fossa and flowed laterally outward. This eruption is interpreted to be caused by rift zone volcanism and lava spread in the surrounding region where SHARAD detects the basal interfaces of these lava units (Figure 3A). Therefore, the Mangala Fossa formation process can be described as the result of rift zone volcanism, where the process may be initiated by surface stretching due to tectonic stress. This process may weaken the upper crust, which could be exploited by later extrusive activities and widen the stretch.

5.3.2 Scenario of reflection in the Labeatis Fossa

Wilson and Head, (2002) found that the observed strain in the Tempe region could be the result of dike emplacement, in which vertical over-pressurized magma filled cracks tens to hundreds of meters in width creating extensional stresses that propagated to form graben. Using this inference, two possible processes to get magma on the surface can be thought off: either fractures caused by the extensional tectonic stresses channeled the magma to the surface (Mege et al., 2003) or a consistent force

from the intrusive dikes triggered the upwards movements of the plume against the base of a plate, forming a conduit for the magma to reach the surface (DiPietro A. J., 2018). In either cases, magma channeled through the graben system. These processes can be tested through the SHARAD detections in the Labetis Fossa, but before that, it is imperative to examine the geologic setup around the reflection area.

About 50 km west of the reflection site in Labeatis Fossa, crater ejecta overlays the fossa floor (Figure 5.6). The presence of ejecta establishes a chronology of events as follows: fossa formation and lava deposition were the earliest activities. The crater formation with overlapping ejecta occurred subsequently. The presence of crater ejecta without embayment at the fossa floor suggest that the fossa floor didn't experience any resurfacing after the crater formation. This geologic setup confirms that the subsurface lava unit was present before the crater formation and may be formed during the fossa formation.

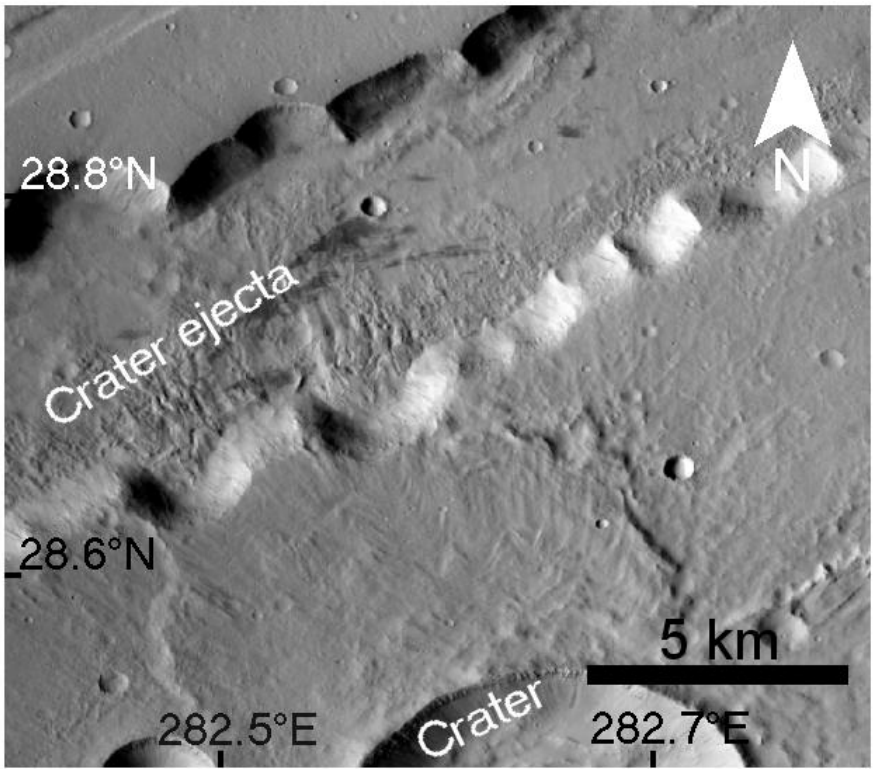

Figure 5.6 CTX image of crater ejecta at the floor of Labeatis Fossa. Crater ejecta without embayment at the fossa floor provides a relative timeline of events.

SHARAD detection of subsurface reflections within Labeatis Fossa has a loss tangent in the range of 0.01 to 0.03, consistent with high-density basalt. The topography of the reflection is sub-horizontal. So, unlike other Tharsis lava flows, flow signatures are not visible at the surface in high resolution images. The low relief is also evident from the minimal variation in the measured time delay of the subsurface reflector (Figure 5.3B). Sub-horizontal topography, derived loss-tangent equivalent to lava, and numerous reflections near a narrow range, which is surrounded by the fossa rim (Figure 5.3B), suggest the existence of a lava pond that cooled and solidified after extruding onto the surface. Previous studies (Wilson and

Head, 2002) suggest that the lava pond may have been formed as a consequence of consistent force of dikes into the over-pressurized magma-filled graben.

Based on the SHARAD detection of subsurface basaltic units and previous studies, it has been concluded that the Labeatis Fossa formation process may be initiated by crustal fault due to regional extension and dikes emplacement. In this process, the fractures caused by the extensional stresses and expansion of dikes channeled the magma from over-pressurized magma filled graben to the fossa surface (Mege and Masson, 1996; Mege et al., 2003) and created a linear crack. The presence of subsurface basaltic units, which are channeled through the magma chamber to the surface of fossa, suggests that magmatism has a prominent role during the formation of Labeatis Fossa.

6 Conclusions

Using SHARAD data, this study presents the first-ever confirmation of the subsurface reflections associated with the Tharsis graben systems. The power attenuation rate and derived loss tangent of the subsurface units are consistent with measured values for Martian basalt. This study supports the previous geological observation that the formation of Mangala Fossa and Labeatis Fossa could be the result of both, tectonic and magmatic processes. The SHARAD based study, here, confirms that magmatism was involved during the formation process of these two graben systems. This study also demonstrates the significance of using high-resolution shallow radar to probe the Martian graben systems and signifies the need for more advanced radar investigations in future missions.

Chapter 6

Summary and Future Prospects

6.1 Summary

The thesis emphasizes on studying the subsurface and surface of Tharsis, the major volcanic region on Mars. Two major geological features have been studied in this thesis: infilled craters and graben systems. In addition to the voluminous basalts, basically, these two features are prominently present in the Tharsis region; therefore, it is important to understand their formation. Most of the previous studies utilized remote sensing based surface geological signatures to understand their formation processes. But this study integrates the surface information derived from orbital imaging with the subsurface information derived from high resolution orbital radar sounding to substantiate the formation process of these important geological features. Two case studies have been examined in detail in this thesis using data from SHARAD, a shallow RADAR sounder onboard MRO. These include the study of subsurface interfaces inside a 65 km~ diameter Lal crater and investigation of the graben system across the Tharsis Montes.

In radar study, it is very important to constrain the geophysical properties of the subsurface material. For this purpose, a model setup is needed to understand the geophysical properties of the completely buried material, as in the case of Lal crater. Therefore, a three-layer model has been developed to constrain the dielectric properties of the material which are entirely buried. In this model, an assumption has been made that the subsurface material is sandwiched between two lava layers, i.e., the upper and bottom layers are lava-infilled. The transmitted wave signal through the top layer acts as incident signal for the subsurface and bottom lava unit. The coefficient of reflection for combined units of subsurface layer and bottom

lava unit is calculated using the linear theory of electromagnetic (*em*) wave propagation having linear polarization and normal incidence. SHARAD observations have been used in this model to measure the power ratio (P_{ss}/P_s) along the track. With the measured value of (P_{ss} / P_s) and assumed dielectric constants of the top and basal unit, this model determines the dielectric constant of the subsurface material. This model can also be used in other regions on Mars where such type of geological setup of subsurface material exists.

Using the above model and other observations, the first study suggests that at least one layer of buried material in the Lal crater has low loss tangent and low dielectric values. The measured loss tangent value is in the range of 0.008-0.009 and has a mean dielectric value of the material is ~5.35. The derived loss tangent and dielectric values are consistent with sedimentary origin hypothesis and also with the cited morphological evidence of the past geological activities in this region. In contrast to the primary lava emplacement in the Tharsis region, the Mangala Fossa region has experienced episodes of both lava flow and erosion that deposited sediments in a large basin. This study demonstrate that a significant quantity of the sedimentary material is buried by lava units in the Lal crater. Thus, the study of the infilling of the Lal crater confirms that the Tharsis region is dominated not only by volcanic activities but also by fluvial activities.

The second study deals with the study of the formation of the graben systems, which shapes the entire Tharsis region. Two hypotheses emerged from the earlier studies for the formation process of these graben systems: i) tectonic process (crustal extension) only, and ii) magmatic and tectonic

processes (where extension and dikes both are involved). In this study, SHARAD data has been used for the first time to decipher the formation process of these two graben systems. The subsurface basaltic unit at the rim of Mangala Fossa and at the floor of Labeatis Fossa supports the hypothesis that along with tectonism, magmatism is also involved in the formation process of these graben systems. This study is trying to end a long debated issue about the origin of these graben systems, at least this study has settled the formation process of these two major graben systems in the Tharsis region.

6.2 Future Directions:

The work presented in this thesis has revealed that the Tharsis region of Mars evolved through diversified geological activities. There were water-related activities in the Mangala crater and the study of Mangala Fossa and Labeatis Fossa revealed that volcanic process was involved in the formation of these graben systems. The two studies described here open a new opportunity for researchers to look into the volcanic regions of Mars beyond the study of only lava cover. The major outflow channels are present in this region, and researchers suggest that these outflow channels are the result of an outburst of water from the cryosphere, which was confined in the subsurface. However, till now, evidence for subsurface ice or water eludes the researchers. A remarkable discovery can be made if geophysical evidence of subsurface ice or water is found through the SHARAD data in this mid latitude region.

The studies carried out in this thesis can be extended to other regions of Tharsis and beyond to study the mechanism of infilling and graben formation elsewhere on Mars. A very good coverage of SHARAD is available for the global Mars. Their studies, similar to the ones carried out in this thesis, will provide a comprehensive understanding of the infilling mechanisms and volcano-tectonic activities on Mars.

6.3 What's next?

It cannot be ascertained, what might be learned from the future mission to Mars, but certainly there will be continued exploration of the Red Planet via diverse multinational spacecraft, orbiters, landers, and rovers during the coming decade. The robotic effort by the United States is undertaken by NASA's Mars Exploration Program (NASA, 2020a) and proposed lander mission by ISRO, which has goals to understand the formation and evolution of Mars. The focus will be to decode the history of geological and climate processes that have shaped Mars through time, the potential for Mars to have hosted life, the future exploration of Mars by human, and how Mars compares to and contrasts with Earth. The study of volcanic terrains directly addresses these goals, and knowledge of Mars's volcanic history, including the heat associated with recent volcanic deposits, may contribute to the search for areas on Mars that may have been capable of supporting life in the past.

Appendix A

List of SHARAD Data

Lal crater

2528001	2549101	2570201
2591301	2599201	2612401
2618301	2648001	2662501
2683601	2768001	2789101
2795701	2816801	3213701
3306001	3412801	3433901
3455001	3490601	3547301
3582901	3631701	3667301
3681801	3724001	3772102
3787301	3973901	4003601
4030601	4273901	

Mangala and Labeatis Fossa

2549101	2570201	2591301
2612401	2618301	2648001
2795701	2816801	3213701
3306001	3455001	3490601
3547301	3631701	3667301
3724001	3772102	3787301
3973901	4003601	4030601
4237901	1588802	1590801
1817601	2233601	2658202
2805901		

References

Alberti, G., Castaldo, L., Orosei, R., Frigeri, A., and Cirillo, G. (2012), Permittivity estimation over Mars by using SHARAD data: the Cerberus Palus area, J. Geophys. Res., 117, E09008, doi:10.1029/2012JE004047

Anderson, R. C., J. M. Dohm, M. P. Golombek, A. F. C. Haldemann, B. J. Franklin, K. L. Tanaka, J. Lias, and B. Peer (2001), Primary centers and secondary concentrations of tectonic activity through time in the western hemisphere of Mars, *J. Geophys. Res.*, 106(E9), 20563–20585, doi:10.1029/2000JE001278.

Arvidson, R E, Morphologic classification of Martian craters and some implications, Icarus, Volume 22, Issue 3,1974, Pages 264-271, ISSN 0019-1035, https://doi.org/10.1016/0019-1035(74)90176-6.

Baker, V. R., G. Komatsu, T. J. Parker, V. C. Gulick, J. S. Kargel, and J. S. Lewis (1992), Channels and valleys on Venus: Preliminary analysis of Magellan data, *J. Geophys. Res.*, 97(E8), 13421–13444, doi:10.1029/92JE00927.

Banerdt, W. B., M. P. Golombek, and K. L. Tanaka, Stress and tectonics on Mars, in Mars, edited by H. H. Kieffer et al., chap. 8, pp. 249 – 297, Univ. of Ariz. Press, Tucson, 1992

Bains Jay, Has Mars become the new space Race? And are we able to justify space Exploration? REACH, Volumes 27–28, 2022, 100049, ISSN 2352-3093, https://doi.org/10.1016/j.reach.2022.100049.

Bamberg, M., Jaumann, R., Asche, H., Kneissl, T., and Michael, G. G. (2014), Floor-Fractured Craters on Mars – Observations and Origin. Planetary and Space Science, 98, 146-162

Bharti, R.B., Smith, I.B., Mishra, S.K., Srivastava, N., Shukla, S.H., , SHARAD detection of sedimentary infilling within an unnamed crater near Mangala Fossa region, Mars, Icarus, Volume 371, 2022, 114713, ISSN 0019-1035, https://doi.org/10.1016/j.icarus.2021.114713.

Byrne S., The Polar Deposits of Mars,2009, Annual Review of Earth and Planetary Sciences, 535-560, 37, 1, 10.1146/ annurev.earth. 031208. 100 101

Cabrol, N.A., Grin, E.A., Distribution, Classification, and Ages of Martian Impact Crater Lakes, Icarus, Volume 142, Issue 1, 1999, Pages 160-172, ISSN 0019-1035, https://doi.org/10.1006/icar.1999.6191.

Campbell, M. J., and J. Ulrichs (1969), Electrical properties of rocks and their significance for lunar radar observations, J. Geophys. Res., 74, 5867–5881, doi: 10.1029/JB074i025p05867.

Campbell, B., Carter, L., Phillips, R., Plaut, J., Putzig, N., Safaeinili, A., Seu, R., Biccari, D., Egan, A., and Orosei, R. (2008), SHARAD radar sounding of the Vastitas Borealis Formation in Amazonis Planitia, J. Geophys. Res., 113, E12010, doi: 10.1029/2008JE003177.

Carr M.H., Volcanism on Mars, J. Geophys. Res., 78 (20) (1973), pp. 4049-4062

Carr, M. H. (1976), "The Volcanoes of Mars." Scientific American, Vol. 234, No. 1, January, 1976, pp. 3243.

Carr M.H.,Clow G.D., Martian channels and valleys: Their characteristics, distribution, and age, Icarus, Volume 48, Issue 1,1981, Pages 91-117, ISSN 0019-1035, https://doi.org/10.1016/0019-1035(81)90156-1.

Carr, M. H. & Head, J. W. Geologic history of Mars. Earth Planet. Sci. Lett. 294, 185–203 (2010).
Carr, M. H., and Schaber, G. G. (1977), Martian permafrost features, *J. Geophys. Res.*, 82(28), 4039– 4054, doi:10.1029/JS082i028p04039.

Carrier, W. D., G. R. Olhoeft, and W. Mendell (1991), Physical properties of the lunar surface, in The Lunar Sourcebook, edited by G. Heiken, D. T. Vaniman, and B. M. French, pp. 475– 594, Cambridge Univ. Press, New York.

Carter, L. M., Campbell, B. A., Holt, J. W., Phillips, R. J., Putzig, N. E., Mattei, S., Seu, R., Okubo, C. H., and Egan, A. F. (2009). Dielectric properties of lava flows west of Ascraeus Mons, Mars. Geophys. Res. Lett., 36, L23204. doi:10.1029/2009GL041234.

Cattermole, P., 1987. Sequence, rheological properties, and effusion rates of volcanic flows at Alba Patera, Mars. J. Geophys. Res. 92 (4), E553-E560.

Cattermole, P. J. (2001). Mars: The Mystery Unfolds (pp.186). Tokyo: Terra.

Christensen, P.R., Eeolian intracrater deposits on Mars: Physical deposits and global distribution. Icarus, 56,496-518, 1983

Christensen, P. R. (1986). Regional dust history on Mars: Physical properties, age, and history, Journal of Geophysical Research, Vol. 91, No. B3, Pages 3533-3545, March 10, 1986

Christensen, P.R., Jakosky, B.M., Kieffer, H.H., Malin, M.C., McSween, Jr., H.Y., Nealson, K., Mehall, G.L., Silverman, S.H., Ferry, S., Caplinger, M., Ravine, M., 2004. The Thermal Emission Imaging System (THEMIS) for

the Mars 2001 Odyssey Mission. Space Science Reviews 110, 85–130. https://doi.org/10.1023/B:SPAC.0000021008.16305.94
Choudhary, P., Holt, J.W., Kempf, S.D. (2016). Surface Clutter and Echo Location Analysis for the Interpretation of SHARAD Data From Mars. IEEE Geoscience and Remote Sensing Letters, 13, 1285-1289. https://doi.org/10.1109/LGRS.2016.2581799

Courville, Samuel W. and Perry, Matthew R. and Putzig, Nathaniel E., Lower Bounds on the Thickness and Dust Content of Layers within the North Polar Layered Deposits of Mars from Radar Forward Modeling (2021). https://app.dimensions.ai/details/publication/pub.1135543132, https://doi.org/10.3847/psj/abda50

Crumpler L.S. and Aubele J. C., 1978, Structural Evolution of Arsia Mons, Pavonis Mons, and Ascreus Mons: Tharsis Region of Mars, Icarus 34, 496-511

Cyril Grima , 2011, PhD thesis, Study of the surface and the on the subsurface of Mars sounding radar: Analysis of data Sharad/MRO

De Hon, R.A., 1992, Martian Lake Basins and Lacustrine Plains, Earth, Moon, and Planets,56, 95-122.

De Hon, R.A., 2010, Hydrologic provinces of Mars: Physiographic controls on drainage and ponding, N.A. Cabrol, E.A. Grin (Eds.), Lakes on Mars, Elsevier, Oxford, pp. 69-89

D.H. Scott, K.L. Tanaka, Mars: paleostratigraphic restoration of buried surfaces in Tharsis Montes, Icarus, 45 (1981), pp. 304-319, 10.1016/0019-1035(81)90036-1

Ernst, R.E., et al. (2001), Giant Dike Swarms: Earth, Venus, and Mars, Ann. Rev. Earth Planet. Sci., 29(1), 489-534

Fassett, C. I., and J. W. Head III (2005), Fluvial sedimentary deposits on Mars: Ancient deltas in a crater lake in the Nili Fossae region, Geophys. Res. Lett., 32, L14201, doi:10.1029/2005GL023456.

Feldman, W. C., et al. (2004), Global distribution of near-surface hydrogen on Mars, *J. Geophys. Res.*, 109, E09006, doi:10.1029/2003JE002160.

Fergason, R. L, Hare, T. M., & Laura, J. (2018). HRSC and MOLA Blended Digital Elevation Model at 200m v2. Astrogeology PDS Annex, U.S. Geological Survey. http://bit.ly/HRSC_MOLA_Blend_v0

French, Bevan M. (1998). "Ch 5: Shock-Metamorphosed Rocks (Impactites) in Impact Structures". Traces of Catastrophe: A Handbook of Shock-Metamorphic Effects in Terrestrial Meteorite Impact Structures. Houston: Lunar and Planetary Institute. pp. 74–78.

Ghatan, G. J., Head, J. W., Wilson, L., and Leask, H. J. (2004). Mangala Valles, Mars: Investigations of the source of flood water and early stages of flooding. Lunar Planet. Sci. [CD-ROM], XXXV, Abstract 1147.

Gurevich, A. V. (1978). Nonlinear phenomena in the ionosphere. Berlin: Springer-Verlag.

Hartmann, W.K., Neukum, G. Cratering Chronology and the Evolution of Mars. *Space Science Reviews* 96, 165–194 (2001). https://doi.org/ 10. 1023/A:1011945222010

Head, J. W., and L. Wilson (2001), Mars: Geological setting of magma/H2O interactions, Lunar Planet. Sci. [CD-ROM], XXXII, Abstract 1215.

Head, J.W., Greeley, R., Golombek, M.P., Hartmann, W.K., Hauber, E., Jaumann, R., Masson, P., Neukum, G., Nyquist, L.E. and Carr, M.H., (2001). 'Geological processes and evolution'. Space Science Reviews, 96 (1-4):263-292.

Head, J.W., Wilson, L., Mitchell, K.L., 2003. Generation of recent massive water floods at Cerberus Fossae, Mars by dike emplacement, cryospheric cracking, and confined aquifer groundwater release. Geophys. Res. Lett. 30 (11), 1577. doi:10.1029/2003GL017135.

Head, J. W., Marchant, D. R., and Ghatan, G. J. (2004). Glacial deposits on the rim of a Hesperian-Amazonian outflow channel source trough: Mangala Valles, Mars. Geophys. Res. Lett.,31,L10701, doi:10.1029/2004GL020294

Hodges, C.A. and Moore, H.J. (1994), Atlas of Volcanic Landforms on Mars, Professional Paper No 1534. Washington, DC: US Geological Survey

Holt, J.W. et al. ,Radar Sounding Evidence for Buried Glaciers in the Southern Mid-Latitudes of Mars.Science322,1235-1238(2008).DOI:10.1126/science.1164246

Hoover, R. H., Robbins, S. J., Putzig, N. E., Riggs, J. D., & Hynek, B. M. (2021). Insight into formation processes of layered ejecta craters on Mars from thermophysical observations. *Journal of Geophysical Research: Planets*, https://doi.org/10.1029/2020JE006801

Hynek, B. M., Beach, M., and Hoke, M. R. T. (2010), Updated global map of Martian valley networks and implications for climate and hydrologic processes, *J. Geophys. Res.*, 115, E09008, doi:10.1029/2009JE003548

Jaumann, R., Tirsch, D., Hauber, E., Ansan, V., di Achille, G., Erkeling, G., Fueten, F., Head, J., Kleinhans, M. G., Mangold, N., Michael, G. G., Neukum, G., Pacifici, A., Platz, T., Pondrelli, M., Raack, J., Reiss, D., Williams, D. A., Adeli, S., Baratoux, D., de Villiers, G., Foing, B., Gupta, S., Gwinner, K., Hiesinger, H., Hoffmann, H., Deit, L. L., Marinangeli, L., Matz, K. D., Mertens, V., Muller, J. P., Pasckert, J. H., Roatsch, T., Rossi, A. P., Scholten, F., Sowe, M., Voigt, J., & Warner, N. (2015). Quantifying geological processes on Mars—Results of the High Resolution Stereo Camera (HRSC) on Mars Express. Planetary and Space Science, 112, 53–97. https://doi.org/10.1016/j.pss.2014.11.029

Kite, Edwin S., Mayer, David P., Wilson, Sharon A., Davis, Joel M., Lucas, Antoine S., Stucky de Quay, Gaia (2019), Persistence of intense, climate-driven runoff late in Mars history, Sci. Adv.5, eaav7710, DOI: 10.1126/sciadv.aav7710

Lalich, D.E., Holt, J.W., Smith, I.B., (2019), Radar Reflectivity as a Proxy for the Dust Content of Individual Layers in the Martian North Polar Layered Deposits. Journal of Geophysical Research: Planets 124, 1690–1703. https://doi.org/10.1029/2018JE005787

Leask, H. J. (2005), Volcano-ice interactions and related geomorphology at Mangala Valles and Aromatum Chaos, Mars. M.Ph. thesis, 199 pp., Lancaster Univ., Lancaster, U. K.

Leask, H. J., Wilson, L., and Mitchell K. L. (2007). Formation of Mangala Fossa, the source of the Mangala Valles, Mars: Morphological development as a result of volcano-cryosphere interactions. J. Geophys. Res., 112, E02011, doi:10.1029/2005JE002644.

Lee, S. W., P. C. Thomas, and J. Veverka, Wind streaks in Tharsis and Elysium: Implications for sediment transport by slope winds, J. Geophys. Res., 87, 10,025-10,042, 1982.

L.L. Tornabene, V. Ling, G.R. Osinski, J.M. Boyce, T.N. Harrison, A.S. McEwen A Revised Global Depth-Diameter Scaling Relationship for Mars Based on Pitted Impact Melt-Bearing Craters LPI, 1719 (2013), p. 2592

Masursky, Harold, Batson, R.M., McCauley, J.F., Soderblom, L.A., Wildey, R.L., Carr, M.H., Milton, D.J., Wilhelms, D.E., Smith, B.A., Kirby, T.B., Robinson, J.C., Leovy, C.B., Briggs, G.A., Young, A.T., Duxbury, T.C., Acton, C.H. Jr., Murray, B.C., Cutts, J.A., Sharp, R.P., Smith, S., Leighton, R.B., Sagan, Carl, Veverka, Joseph, Noland, M., Lederberg, Joshua, Levinthal, E., Pollock, J.B., Moore, J.T., Jr., Hartmann, W.K., Shipley, E.N., de Vaucouleurs, G., and Davies, M.E., 1972, Mariner 9 television reconnaissance of Mars and its satellites; preliminary results: Science, v. 175, no. 4019, p. 294-305.

McCauley, J. F. (1973), Mariner 9 evidence for wind erosion in the equatorial and mid-latitude regions of Mars, *J. Geophys. Res.*, 78(20), 4123–4137, doi:10.1029/JB078i020p04123.

McCauley J.F., M.H. Carr, J.A. Cutts, W.K. Hartmann, Harold Masursky, D.J. Milton, R.P. Sharp, D.E. Wilhelms, Preliminary mariner 9 report on the geology of Mars, Icarus, Volume 17, Issue 2, 1972, Pages 289-327, ISSN 0019-1035, https://doi.org/10.1016/0019-1035(72)90003-6.

McDowell, M. L., and V. E. Hamilton (2007), Geologic characteristics of relatively high thermal inertia intracrater deposits in southwestern Margaritifer Terra, Mars, J. Geophys. Res., 112, E12001, doi:10.1029/2007JE002925.

McEwen, A., Malin, M., Carr, M. et al. Voluminous volcanism on early Mars revealed in Valles Marineris. Nature 397, 584–586 (1999).

McGetchin, T. R., M. Settle, and J. W. Head (1973), Radial thickness variation in impact crater ejecta: Implications for lunar basin

deposits, Earth Planet. Sci. Lett., 20, 226– 236, doi:10.1016/0012-821X(73)90162-3.S.

McKay CP, Stoker CR. The early environment and its evolution on Mars: Implication for life. Rev Geophys 1989;27(2):189; doi: 10.1029/RG027i002p00189

Mège, D., and Masson, P., (1996). A plume tectonics model for the Tharsis province, Mars: Planetary and Space Science, v. 44p. 1499-1546

Mège, D., et al. (2003). Volcanic rifting at Martian grabens, J. Geophys. Res., 108(E5), 5044

Melosh H. J. (1989) Impact Cratering: A Geologic Process. Oxford Univ., New York. 245 pp

Morgan, G.A., Campbell, B.A., Carter, L. M., Plaut, J. J. 2015. Evidence for the episodic erosion of the Medusae Fossae Formation preserved within the youngest volcanic province on Mars. Geophys. Res. Lett. 42, 7336-7342, https:// doi.org/10.1002/2015GL065017

Mouginot, J., A. Pommerol, P. Beck, W. Kofman, and S. M. Clifford (2012), Dielectric map of the Martian northern hemisphere and the nature of plain filling materials, *Geophys. Res. Lett.*, 39, L02202, doi:10.1029/2011GL050286.

Newsom, H. E., G. E. Brittelle, C. A. Hibbitts, L. J. Crossey, and A. M. Kudo (1996), Impact crater lakes on Mars, J. Geophys. Res., 101(E6), 14951–14955, doi:10.1029/96JE01139.

Orosei R., Jordan R.L., Morgan D.D., Cartacci M., Cicchetti A., Duru F., Gurnett D.A., Heggy E., Kirchner D.L., Noschese R., Kofman W., Masdea A., Plaut J.J., Seur.R, Watters T.R., Picardi G., Mars Advanced Radar for

Subsurface and Ionospheric Sounding (MARSIS) after nine years of operation: A summary, Planetary and Space Science, Volume 112,2015, https://doi.org/10.1016/j.pss.2014.07.010.

Phillips RJ, Zuber MT, Solomon SC, Golombek MP, Jakosky BM, Banerdt WB, Smith DE, Williams RM, Hynek BM, Aharonson O, Hauck SA 2nd. Ancient geodynamics and global-scale hydrology on Mars. Science. 2001 Mar 30;291(5513):2587-91. doi: 10.1126/science.1058701. Epub 2001 Mar 15. PMID: 11283367.

Phillips RJ. *et al.,* Mars North Polar Deposits: Stratigraphy, Age, and Geodynamical Response. *Science* 320, 1182-1185(2008). DOI:10.1126/science.1157546

Platz Thomas, Gregory Michael, Eruption history of the Elysium Volcanic Province, Mars, Earth and Planetary Science Letters, Volume 312, Issues 1–2,2011, Pages 140-151, ISSN 0012-821X, https://doi.org/10.1016/j.epsl.2011.10.001.

Plaut, J. J., Safaeinili, A., Holt, J. W., Phillips, R. J., Head, J. W., Seu, R., Putzig, N. E., and Frigeri, A. (2009), Radar evidence for ice in lobate debris aprons in the mid-northern latitudes of Mars, Geophys. Res. Lett., 36, L02203, doi:10.1029/2008GL036379.

Plescia, J. B., and R. S. Saunders,(1982). Tectonic history of the Tharsis region, Mars, J. Geophys. Res., 87, 9775–9791, 1982.

Pondrelli, M., A. Baliva, S. Di Lorenzo, L. Marinangeli, and A. P. Rossi (2005), Complex evolution of paleolacustrine systems on Mars: An example from the Holden crater, *J. Geophys. Res.*, 110, E04016, doi:10.1029/2004JE002335.

Putzig NE, Phillips RJ, Campbell BA, Holt JW, Plaut JJ, Carter LM, Egan AF, Bernardini F, Safaeinili A, Seu R, Subsurface structure of Planum Boreum from Mars Reconnaissance Orbiter Shallow Radar soundings, Icarus, Volume 204, Issue 2, 2009, Pages 443-457, ISSN 0019-1035, https://doi.org/10.1016/j.icarus.2009.07.034.

Putzig, N. E., Phillips, R. J., Campbell, B. A., Plaut, J. J., Holt, J. W., Bernardini, F., Egan, A. F., Smith, I. B., 2016. Custom SHARAD processing via the CO-SHARPS Processing Boutique. LPSC XLVII, Abstract 3010.

Putzig, N. E., Seu R., Morgan G.A., Smith I.B., Campbell B.A., Perry M.R., Marco M., Science results from sixteen years of MRO SHARAD operations, Icarus, 2023, 115715, ISSN 0019-1035, https://doi.org/10.1016/j.icarus.2023.115715.

Scott, D. H., and K. L. Tanaka, (1986) Geologic map of the western equatorial region of Mars, U.S. Geol. Surv. Misc. Invest. Ser.Map, I-1802-A, scale 1:15,000,000

Scott, E., and L. Wilson (2002). Plinian eruptions and passive collapse events as mechanisms of formation for Martian pit chain craters, J. Geophys. Res., 107(E4), 5020, 10.1029/2000JE001432.

Schneeberger, D.M., Pieri, D.C., 1991. Geomorphology and stratigraphy of Alba Patera, Mars. J. Geophys. Res. 96 (2), 1907-1930. https://doi.org/10.1029/90JB01662

Schultz R. A., Chris H. Okubo, Cheryl L. Goudy, Scott J. Wilkins.(2004). Igneous dikes on Mars revealed by Mars Orbiter Laser Altimeter topography. *Geology* ; 32 (10): 889–892. 10.1130/G20548.1

Seu, R., Biccari, D., Orosei, R., Lorenzoni, L. V., Phillips, R. J., Marinangeli, L., Picardi, G., Masdea, A., & Zampolini, E. (2004). SHARAD: The MRO 2005 Shallow radar. Planetary and Space Science, 52(1-3), 157– 166.

Seu, R., Phillips, R. J., Biccari, D., Orosei, R., Masdea, A., Picardi, G., Safaeinili, A., Campbell, B. A., Plaut, J. J., Marinangeli, L., Smrekar, S. E., & Nunes, D. C. (2007). SHARAD sounding radar on the Mars Reconnaissance Orbiter. J. Geophys. Res.112, E05S05. https:// doi.org/ 10.1029/2006 JE002745

Simon, M. N., Carter, L. M., Campbell, B. A., Phillips, R. J., and Mattei, S. (2014), Studies of lava flows in the Tharsis region of Mars using SHARAD, J. Geophys. Res. Planets, 119, 2291– 2299. doi:10.1002/2014JE004666.

SHARP R.P., MALIN M.C.; Channels on Mars. GSA Bulletin 1975;; 86 (5): 593–609. doi: https://doi.org/10.1130/0016-7606(1975) 86<593:COM> 2.0.CO;2

Shoemaker, E. S., Carter, L. M., Garry, W. B., Morgan, G. A., & Plaut, J. J. (2022). New insights into subsurface stratigraphy northwest of Ascraeus Mons, Mars, using the SHARAD and MARSIS radar sounders. *Journal of Geophysical Research: Planets*, 127, e2022JE007210. https://doi.org/10.1029/2022JE007210

Simon, M. N., Carter, L. M., Campbell, B. A., Phillips, R. J., and Mattei, S. (2014), Studies of lava flows in the Tharsis region of Mars using SHARAD, *J. Geophys. Res. Planets*, 119, 2291– 2299. doi:10.1002/2014JE004666.

Smith, D. E., Zuber, M. T., Frey, H. V., Garvin, J. B., Head, J. W., Muhleman, D. O., Pettengill, G. H., Phillips, R. J., Solomon, S. C., Zwally, H. J., Banerdt, W. B., Duxbury, T. C., Golombek, M. P., Lemoine, F. G., Neumann, G. A., Rowlands, D. D., Aharonson, O., Ford, P. G., Ivanov, A. B., Johnson, C. L.,

McGovern, P. J., Abshire, J. B., Afzal, R. S., & Sun, X. (2001). Mars Orbiter Laser Altimeter: Experiment summary after the first year of global mapping of Mars. *J. Geophys. Res.*, 106(E10), 23,689–23,722. https://doi.org/10.1029/2000JE001364

Smith, I. B., and J. W. Holt (2015), Spiral trough diversity on the north pole of Mars, as seen by Shallow Radar (SHARAD), J. Geophys. Res. Planets, 120, 362–387, doi: 10.1002/2014JE004720

Squyres, S. W., S. M. Clifford, R. O. Kuzmin, J. R. Zimbelman, and F. M. Costard (1992), Ice in the Martian regolith, in Mars, edited by H. H. Kieffer et al., pp. 523– 554, Univ. of Ariz. Press, Tucson.

Smrekar, S., and C.M. Pieters, Near-infrared spectroscopy of probable impact melt from three large lunar highland craters, Icarus, 63, 442-452, 1985

T. Platz, G. Michael, Eruption history of the Elysium volcanic province, Mars, Earth Planet Sci. Lett., 312 (2011), pp. 140-151, 10.1016/j.epsl.2011.10.001

Tanaka, K. L., and Chapman, M. G. (1990). The relation of catastrophic flooding of Mangala Valles, Mars, to faulting of Memnonia Fossae and Tharsis volcanism. J. Geophys. Res., 95, 14,315–14,323.
Tanaka, K. L., D. H. Scott, and R. Greeley,(1992). Global stratigraphy, in Mars, edited by H. H. Kieffer et al., pp. 345 – 382, Univ. of Ariz. Press, Tucson

Tanaka, K.L., Skinner, J.A., Jr., Dohm, J.M., Irwin, R.P., III, Kolb, E.J., Fortezzo, C.M., Platz, T., Michael, G.G., and Hare, T.M., 2014, Geologic map of Mars: U.S. Geological Survey Scientific Investigations Map 3292, scale 1:20,000,000, pamphlet 43 p., https://dx.doi.org/10.3133/sim3292

Thomas, P., Veverka, J., Lee, S., and Bloom, A. (1981), Classification of Wind Streaks on Mars, Icarus 45, 124-153

Ulaby, F. T., T. Bengal, J. East, M. C. Dobson, J. Garvin, and D. Evans (1988), Microwave dielectric spectrum of rocks, Rep. 23817-1-T, Univ. of Mich. Radiat. Lab., Ann Arbor.

Wilhelms, D.E., McCauley, J.F., and Trask, N.J.(1987), The geologic history of the Moon, https://doi.org/10.3133/pp1348

Wilson, L., and J. W. Head III, Tharsis-radial graben systems as the surface manifestation of plume-related dike intrusion complexes: Models and implications, *J. Geophys. Res.*, 107(E8), doi:10.1029/2001JE001593, 2002.

Wilson, L., and Head, J. W. (2004). Evidence for a massive phreatomagmatic eruption in the initial stages of formation of the Mangala Valles outflow channel, Mars. Geophys. Res. Lett., 31(15), L15701, doi:10.1029/ 2004GL020322.

Wise, D.U., Golombek, M.P., McGill, G.E., Tharsis province of Mars: geologic sequence, geometry, and a deformation mechanism, Icarus, 38 (456) (1979), p. 472

Wise, D.U., Golombek, M.P., G.E. McGill, G.E., Tectonic evolution of Mars, J. Geophys. Res., 84 (1979), pp. 7934-7939

Wyrick and Smart, 2009, Dike-induced deformation and Martian graben systems J. Volcanol. Geotherm. Res., 10 (2009), pp. 1 11, 10.1016/j.volgeores.2008.11.022

Zimbelman, J. R., Craddock, R. A., Greeley R., and Kuzmin, R. O. (1992). Volatile history of Mangala Valles, Mars. J. Geophys. Res., 97, 18,309–18,317.

Zuber, M. T., The crust and mantle of Mars, Nature, 412, 220 – 227, 2001

List of Publications

1. Rajiv R. Bharti, Isaac B. Smith, S.K. Mishra, N. Srivastava, Shital H. Shukla, 2022, SHARAD detection of sedimentary infilling within an unnamed crater near Mangala Fossa region, Mars, Icarus, https://doi.org/10.1016/j.icarus.2021.114713

2. Rajiv R. Bharti, Isaac B. Smith, Shital H. Shukla , 2023, Subsurface study of the Tharsis graben system using SHARAD (2023) data, Icarus, https://doi.org/10.1016/j.icarus.2023.115681

Conferences/symposiums Abstracts

3. Rajiv R Bharti , Sanjay Mishra, Characterizing the Martian subsurface using Shallow Radar, URSI, AP-RASC, New Delhi, 2019

4. Rajiv R Bharti , Isaac Smith, Study of Subsurface of Lava Province on Mars using SHAllow RADar (SHARAD), IPSC, 2020

5. Rajiv R Bharti , Isaac Smith, Sanjay Mishra, SHARAD detection of subsurface reflection near Mangala Fossa, Mars, IPSC, 2021

6. Rajiv R. Bharti , Isaac B. Smith , S. K. Mishra , N. Srivastava , Shital H Shukla , SHARAD detection of sedimentary infilling within an unnamed crater near Mangala Fossa region, Mars, NSSS 2022

7. Rajiv R. Bharti , Isaac B. Smith, Shital H Shukla, SHARAD Study of the Martian Graben System, IPSC 2022

8. Rajiv R. Bharti , Isaac B. Smith, Shital H Shukla, study of the Tharsis graben system using SHARAD data, IPSC 2023